ACS Photonics

pubs.acs.org/journal/apchd5

Perspective

Perspective on Meta-Boundaries

Xinyan Zhang, Jialin Chen, Ruoxi Chen, Chan Wang, Tong Cai,* Reza Abdi-Ghaleh, Hongsheng Chen,* and Xiao Lin*

Cite This: https://doi.org/10.1021/acsphotonics.2c01705

Read Online

ACCESS | Metrics & More | Article Recommendations

ABSTRACT: The judicious design of the electromagnetic boundary provides a crucial route to control light−matter interactions, and it is thus fundamental to basic science and practical applications. General design approaches rely on the manipulation of bulk properties of the superstrate or substrate and on the modification of boundary geometries. Due to the recent advent of metasurfaces and low-dimensional materials, the boundary can be flexibly featured with a surface conductivity, which can be rather complex but provide an extra degree of freedom to regulate the propagation of light. In this Perspective, we denote the boundary with a nonzero surface conductivity as the meta-boundary. The meta-boundaries are categorized into four types, namely, isotropic, anisotropic, biisotropic, and bianisotropic meta-boundaries, according to the electromagnetic boundary conditions. Accordingly, the latest developments for these four kinds of meta-boundaries are reviewed. Finally, an outlook on the research tendency of meta-boundaries is provided, particularly on the manipulation of light−matter interactions by simultaneously exploiting meta-boundaries and metamaterials.

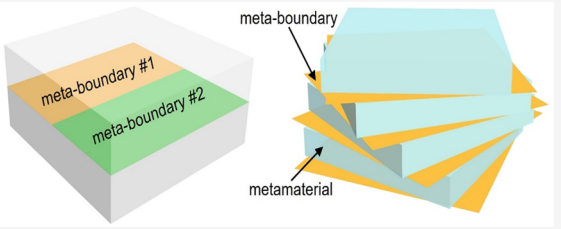

KEYWORDS: *boundary conditions, light−matter interactions, near-field optics, 2D materials, metasurfaces, metamaterials*

INTRODUCTION

When two different bulk media are stacked together, an electromagnetic boundary is formed. The electromagnetic boundary can be exploited to flexibly control the propagation of light, including its phase, amplitude, polarization, and direction.[1−10] This way, the electromagnetic boundary is crucial to control light−matter interactions, and its continuing exploration has led to many exotic phenomena and practical applications, including negative refraction,[11−16] superlens,[17,18] cloak,[19−24] and DB boundary.[19,25,26]

Generally, the design of the electromagnetic boundary relies on changing the geometric shape of the boundary (e.g., grating) or on changing the optical properties of bulk media, which may function as the superstrate or substrate of the boundary. Thanks to the recent development of metamaterials, the optical properties of bulk media can be tailored in a desired manner.[27−35] For instance, by following the design methodology of metamaterials, the effective optical response of bulk media can range from being isotropic, anisotropic, and biisotropic to being bianisotropic,[36−39] and is closely related to Maxwell equations, which are the basis to describe the light−matter interaction. The Maxwell equations are

$$\nabla \times \overline{H} = \partial \overline{D}/\partial t + \overline{J} \tag{1}$$

$$\nabla \times \overline{E} = -\partial \overline{B}/\partial t \tag{2}$$

$$\nabla \cdot \overline{D} = \rho \tag{3}$$

$$\nabla \cdot \overline{B} = 0 \tag{4}$$

where $\overline{J}$ and ρ represent the electric current density and electric charge density, respectively; the relations between the electric field $\overline{E}$, magnetic field $\overline{H}$, electric displacement $\overline{D}$, and magnetic flux density are described by the constitutive relations. That is, the constitutive relations serve as the complementary but important information for Maxwell equations and can well describe the optical response of bulk media. To be specific, the constitutive relations for bulk isotropic media[40] can be readily expressed as

$$\overline{D} = \varepsilon \cdot \overline{E} \tag{5}$$

$$\overline{B} = \mu \cdot \overline{H} \tag{6}$$

where ε and μ represent the permittivity and permeability, respectively. Similarly, the constitutive relations for anisotropic media[40] are written as

$$\overline{D} = \overline{\overline{\varepsilon}} \cdot \overline{E} \tag{7}$$

$$\overline{B} = \overline{\overline{\mu}} \cdot \overline{H} \tag{8}$$

where $\overline{\overline{\varepsilon}}$ and $\overline{\overline{\mu}}$ become a tensor (namely, a 3 × 3 matrix). By contrast, the constitutive relations for biisotropic media[40] are

Special Issue: Photonics in China

Received: November 8, 2022
Revised: February 9, 2023
Accepted: February 16, 2023

$$\bar{D} = \varepsilon \cdot \bar{E} + \xi \cdot \bar{H} \tag{9}$$

$$\bar{B} = \mu \cdot \bar{H} + \zeta \cdot \bar{E} \tag{10}$$

where ξ and ζ describe the magnetoelectric coupling. Similarly, the constitutive relations for bianisotropic media[40] can be expressed as

$$\bar{D} = \bar{\bar{\varepsilon}} \cdot \bar{E} + \bar{\bar{\xi}} \cdot \bar{H} \tag{11}$$

$$\bar{B} = \bar{\bar{\mu}} \cdot \bar{H} + \bar{\bar{\zeta}} \cdot \bar{E} \tag{12}$$

where $\bar{\bar{\xi}}$ and $\bar{\bar{\zeta}}$ become to a tensor. The diversity of bulk media as governed by eqs 5−12 indicates the enormous possibilities to conceive different types of electromagnetic boundaries.

Apart from changing the optical properties of bulk media, the electromagnetic boundary itself can be directly tailored due to the recent advent of metasurfaces[41−45] and low-dimensional materials,[46−53] which can be well modeled by an effective two-dimensional surface without a thickness, but with a nonzero surface conductivity.[54−65] In other words, with the addition of metasurfaces or low-dimensional materials, the boundary can be featured with a nonzero surface conductivity. This way, the judicious design of surface conductivity can provide an extra degree of freedom to regulate the electromagnetic boundary conditions and thus the light-matter interaction. For the simplicity of conceptual illustration in this work, the boundary without surface conductivities is denoted as the common boundary; by contrast, the boundary with nonzero surface conductivities is termed as the meta-boundary; see the schematic in Figure 1a,b.

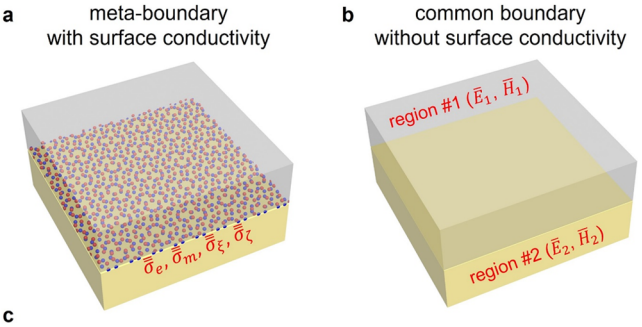

c

boundary conditions of meta-boundaries	
isotropic meta-boundary	$\hat{n} \times (\bar{E}_1 - \bar{E}_2) = \sigma_m \cdot (\bar{H}_1 + \bar{H}_2)/2$ $\hat{n} \times (\bar{H}_1 - \bar{H}_2) = \sigma_e \cdot (\bar{E}_1 + \bar{E}_2)/2$
anisotropic meta-boundary	$\hat{n} \times (\bar{E}_1 - \bar{E}_2) = \bar{\bar{\sigma}}_m \cdot (\bar{H}_1 + \bar{H}_2)/2$ $\hat{n} \times (\bar{H}_1 - \bar{H}_2) = \bar{\bar{\sigma}}_e \cdot (\bar{E}_1 + \bar{E}_2)/2$
biisotropic meta-boundary	$\hat{n} \times (\bar{E}_1 - \bar{E}_2) = \sigma_m \cdot (\bar{H}_1 + \bar{H}_2)/2 + \sigma_\xi \cdot (\bar{E}_1 + \bar{E}_2)/2$ $\hat{n} \times (\bar{H}_1 - \bar{H}_2) = \sigma_e \cdot (\bar{E}_1 + \bar{E}_2)/2 + \sigma_\zeta \cdot (\bar{H}_1 + \bar{H}_2)/2$
bianisotropic meta-boundary	$\hat{n} \times (\bar{E}_1 - \bar{E}_2) = \bar{\bar{\sigma}}_m \cdot (\bar{H}_1 + \bar{H}_2)/2 + \bar{\bar{\sigma}}_\xi \cdot (\bar{E}_1 + \bar{E}_2)/2$ $\hat{n} \times (\bar{H}_1 - \bar{H}_2) = \bar{\bar{\sigma}}_e \cdot (\bar{E}_1 + \bar{E}_2)/2 + \bar{\bar{\sigma}}_\zeta \cdot (\bar{H}_1 + \bar{H}_2)/2$

Figure 1. Meta-boundaries. (a, b) Schematic of meta-boundaries and common boundaries. (c) Boundary conditions for different types of meta-boundaries.

Due to the abundance of metasurfaces and low-dimensional materials, the electromagnetic boundary conditions can have different mathematical forms. According to these different forms of electromagnetic boundary conditions, the meta-boundary in principle can be categorized into four types, namely isotropic, anisotropic, biisotropic and bianisotropic meta-boundaries; see the summarization of boundary conditions for meta-boundaries in Figure 1c. Such categorization for meta-boundaries based on the boundary conditions is intrinsically analogous to the studies for bulk media, whose categorization is based on constitutive relations.

To be specific, the boundary conditions for isotropic meta-boundary are

$$\hat{n} \times (\bar{E}_1 - \bar{E}_2) = \sigma_m \cdot (\bar{H}_1 + \bar{H}_2)/2 \tag{13}$$

$$\hat{n} \times (\bar{H}_1 - \bar{H}_2) = \sigma_e \cdot (\bar{E}_1 + \bar{E}_2)/2 \tag{14}$$

where σ_e and σ_m stand for the electric and magnetic surface conductivities, respectively; $\bar{E}_1$ or $\bar{E}_2$ and $\bar{H}_1$ or $\bar{H}_2$ are the electric and magnetic fields in the superstrate (denoted as region 1 in Figure 1a,b) or substrate (region 2) very close to the boundary, respectively; and $\hat{n}$ is the surface normal.

When the meta-boundary becomes anisotropic, the boundary conditions in eqs 13 and 14 are changed to

$$\hat{n} \times (\bar{E}_1 - \bar{E}_2) = \bar{\bar{\sigma}}_m \cdot (\bar{H}_1 + \bar{H}_2)/2 \tag{15}$$

$$\hat{n} \times (\bar{H}_1 - \bar{H}_2) = \bar{\bar{\sigma}}_e \cdot (\bar{E}_1 + \bar{E}_2)/2 \tag{16}$$

where $\bar{\bar{\sigma}}_e$ and $\bar{\bar{\sigma}}_m$ are tensors (namely, a 2 × 2 matrix).

If the meta-boundary is biisotropic, the magnetoelectric coupling would appear in the boundary conditions. Then the boundary conditions for biisotropic meta-boundary become to

$$\hat{n} \times (\bar{E}_1 - \bar{E}_2) = \sigma_m \cdot (\bar{H}_1 + \bar{H}_2)/2 + \sigma_\xi \cdot (\bar{E}_1 + \bar{E}_2)/2 \tag{17}$$

$$\hat{n} \times (\bar{H}_1 - \bar{H}_2) = \sigma_e \cdot (\bar{E}_1 + \bar{E}_2)/2 + \sigma_\zeta \cdot (\bar{H}_1 + \bar{H}_2)/2 \tag{18}$$

where the surface conductivities of σ_ξ and σ_ζ represent the magnetoelectric coupling.

If the meta-boundary is bianisotropic, the general form for boundary conditions are

$$\hat{n} \times (\bar{E}_1 - \bar{E}_2) = \bar{\bar{\sigma}}_m \cdot (\bar{H}_1 + \bar{H}_2)/2 + \bar{\bar{\sigma}}_\xi \cdot (\bar{E}_1 + \bar{E}_2)/2 \tag{19}$$

$$\hat{n} \times (\bar{H}_1 - \bar{H}_2) = \bar{\bar{\sigma}}_e \cdot (\bar{E}_1 + \bar{E}_2)/2 + \bar{\bar{\sigma}}_\zeta \cdot (\bar{H}_1 + \bar{H}_2)/2 \tag{20}$$

where $\bar{\bar{\sigma}}_\xi$ and $\bar{\bar{\sigma}}_\zeta$ also become tensors.

From eqs 13−20, the meta-boundary provides an exotic way to tailor the electromagnetic boundary conditions and is thus of paramount importance for the exploration of novel light−matter interactions. We then briefly review the recent progress in the realm of meta-boundaries, followed by a perspective on their research tendency. Particularly, due to the infinite vitality of metamaterials and meta-boundaries, the combination of metamaterials and meta-boundaries is promising to provide a powerful platform for the arbitrary manipulation of light.

ISOTROPIC META-BOUNDARY

As indicated in eqs 13 and 14, the isotropic meta-boundary requires the emergence of isotropic electric and magnetic surface conductivities at the boundary. These surface conductivities are typically constructed, for example, by exploiting metal-based metasurfaces[54−63] in Figure 2a−c, all-dielectric metasurfaces,[66−69] monolayer graphene[49,70] in Figure 2d, and the inversion layer at the insulator-semiconductor interface (which acts as a two-dimensional electron gas and is similar to the role of graphene).[71] Moreover, due to the recent

https://doi.org/10.1021/acsphotonics.2c01705
ACS Photonics XXXX, XXX, XXX−XXX

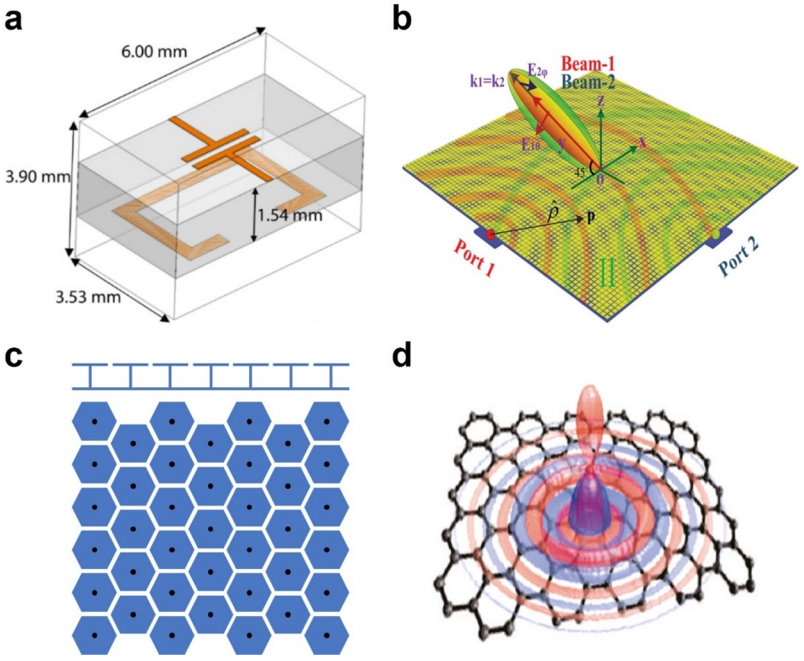

Figure 2. Isotropic meta-boundaries. (a) Unit cell for Huygens' surface, which can be modeled by an electric surface conductivitity and a magnetic conductivitity; reprinted with permission from ref 81. Copyright 2013 American Physical Society. (b) Holographic metasurfaces for dual-functional radiations; reprinted with permission from ref 60. Copyright 2016 Wiley. (c) High impedance metasurface with a mushroom-like unit structure; reprinted with permission from ref 54. Copyright 1999 IEEE. Distributed under a CC BY4.0 license https://creativecommons.org/licenses/by/4.0/. (d) Near-field excitation of graphene plasmons by depositing a dipole close to the graphene; reprinted with permission from ref 49. Copyright 2011 American Chemical Society.

advances in nanofabrication, these surface conductivities based either on metasurfaces or low-dimensional materials can be actively tunable.[72−79]

The elaborate choice of electric and magnetic surface conductivities at the isotropic meta-boundary enables many exotic applications, such as the design of Huygens' surface,[80,81] frequency-selective surface,[82−84] and high-impedance surface. With the existence of Huygens' surface in Figure 2a, the transmitted light can propagate along a direction, which is not normal to the meta-boundary, under the normal incidence.[81] When considering the frequency dispersion of these surface conductivities, the isotropic meta-boundary can be transparent only to light incidence with certain frequencies and functions as a frequency-selective surface. When integrating the isotropic meta-boundary with input ports, the isotropic holographic metasurfaces for dual-functional radiations without mutual interferences can be obtained,[60] as shown in Figure 2b. The high-impedance surface could be built by artificially engineered metal-based structures, such as a mushroom-like unit structure in Figure 2c.[54] For high-impedance surfaces, their equivalent surface conductivity could be obtained by analyzing the associated Floquet modes.[64] For example, if high-impedance surface is constructed by a mesh of ideally conducting strips, the effective surface conductivity for TE waves can be modeled by $\sigma_e^{TE} = i\frac{2\pi c}{\eta_0 wD}\frac{1}{\ln\csc(\pi w/2D)}$,[65] where D is the period of square unit cell, w is the width of metal strips, η_0 is the impedance of free space, and c is the speed of light in free space. Similarly, the effective surface conductivity for TM waves can be characterized by $\sigma_e^{TM} = i\frac{2\pi c}{\eta_0 wD}\frac{1}{\ln\csc(\pi w/2D)}\frac{1}{(1-\sin^2(90^\circ-\theta)/(\varepsilon_r+1))}$,[65] where θ is the incident angle and ε_r is the relative permittivity of the substrate. In addition, while the Brewster effect[40,85−90] for transverse-electric (TE) waves is believed to exist only in systems with magnetic responses, the isotropic meta-boundary with a specific electric surface conductivity can give rise to the TE Brewster effect in a homogeneous dielectric interface without magnetic responses.[85]

The isotropic meta-boundary is also widely used in controlling the light flow at the subwavelength scale, especially for the propagation of surface waves. According to the boundary conditions in eqs 13 and 14, the dispersion for transverse-magnetic (TM) or TE surface waves supported at the isotropic meta-boundary can be derived as

$$\text{TM surface waves: } \left(1+\frac{\sigma_e k_z}{2\omega\varepsilon}\right)\left(1-\frac{\sigma_m k_z}{2\omega\mu}\right)=0 \tag{21}$$

$$\text{TE surface waves: } \left(\frac{k_z}{\omega\mu}+\frac{\sigma_e}{2}\right)\left(\frac{k_z}{\omega\varepsilon}-\frac{\sigma_m}{2}\right)=0 \tag{22}$$

For illustration, here we consider the symmetric structure in Figure 1a, namely, regions 1 and 2 are the same and have a permittivity ε and a permeability μ; and k_z stands for the component of the wave vector perpendicular to the meta-boundary. If the environment is composed of positive-index materials, namely $\varepsilon > 0$ and $u > 0$, the emergence of TM surface waves in isotropic meta-boundaries requires $\mathrm{Im}(\sigma_e) > 0$ and $\mathrm{Im}(\sigma_m) < 0$ according to eq 21; by contrast, the existence condition for TE surface waves in isotropic meta-boundaries becomes to $\mathrm{Im}(\sigma_e) < 0$ and $\mathrm{Im}(\sigma_m) > 0$ according to eq 22.[48]

If the isotropic meta-boundary is composed of monolayer graphene, the spatial confinement of TM graphene plasmons is generally much better than that of TE graphene plasmons.[91−94] For example, the wavelength of TM graphene plasmons (Figure 2d) can be 2 orders of magnitude smaller than the

https://doi.org/10.1021/acsphotonics.2c01705
ACS Photonics XXXX, XXX, XXX−XXX

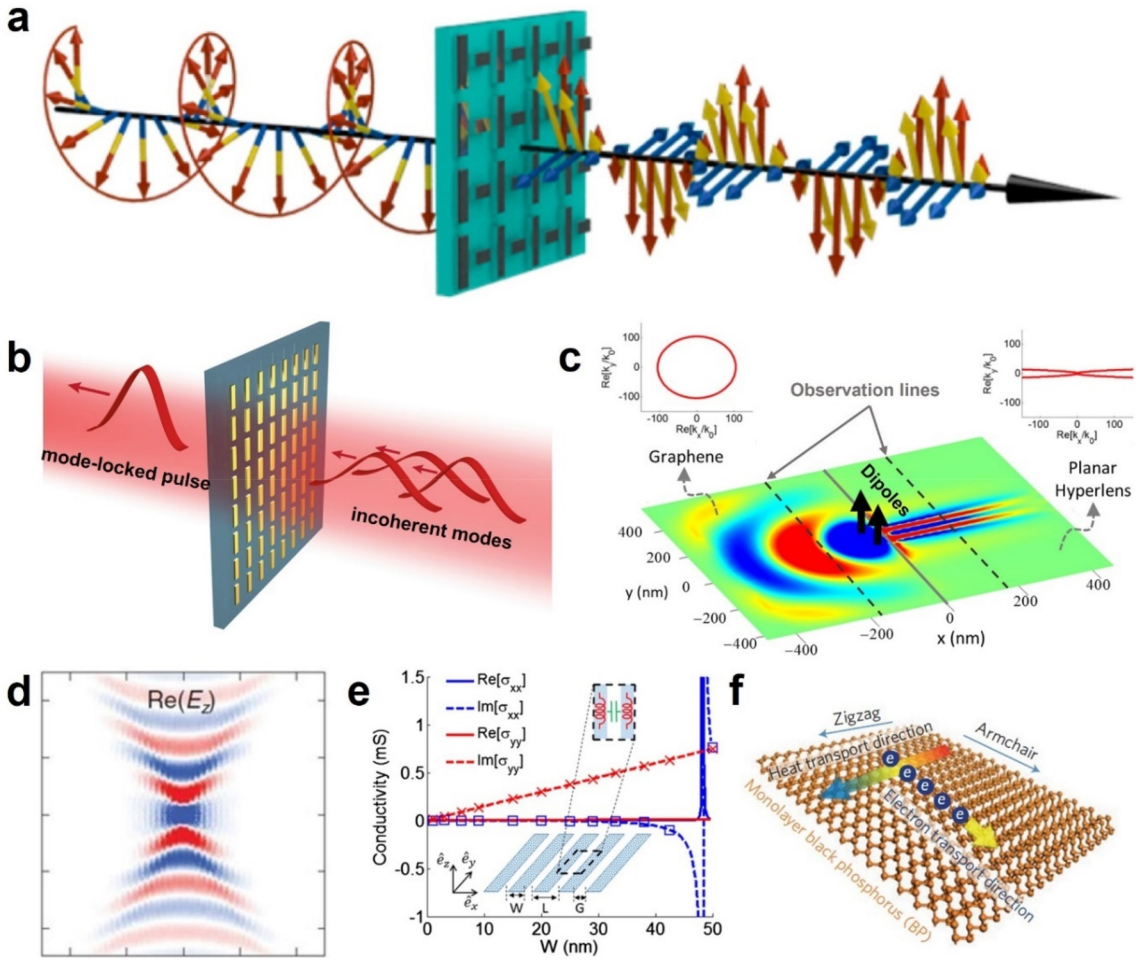

Figure 3. Anisotropic meta-boundaries. (a) Conversion between the circularly polarized light and linearly polarized light by using the anisotropic meta-boundary; reprinted with permission from ref 104. Copyright 2013 American Chemical Society. (b) Plasmonic metasurface with periodically arranged gold nanorods; reprinted with permission from ref 105. Copyright 2020 Springer Nature. Distributed under a CC BY 4.0 license https://creativecommons.org/licenses/by/4.0/. (c) Planar hyperlens. The inset shows the isofrequency contours of surface plasmons in the left and right regions; reprinted with permission from ref 106. Copyright 2016 American Chemical Society. (d) Near-field excitation of surface waves by putting a dipole close to a hyperbolic metasurface; reprinted with permission from ref 46. Copyright 2018 AAAS. (e) Surface conductivity of hyperbolic metasurfaces constructed by graphene nanoribbons; reprinted with permission from ref 110. Copyright 2015 American Physical Society. (f) Monolayer black phosphorus; reprinted with permission from ref 126. Copyright 2014 Springer Nature.

wavelength of light in free space, while the wavelength of TE graphene plasmons is similar to the wavelength of light in free space. Moreover, due to the low material loss and active tunability of graphene, there are extensive studies about TM surface waves in isotropic meta-boundaries with graphene. On the other hand, how to improve the spatial confinement of TE surface waves in isotropic meta-boundaries with graphene, especially in terahertz or infrared regimes, remains a challenging issue. One way to tackle this issue is to replace the positive-index environment of the isotropic meta-boundary with the negative-index environment (which has $\varepsilon < 0$ and $u < 0$).[95] Under this scenario, it is worthy to note that the existence conditions for both TM and TE surface waves in isotropic meta-boundaries would be drastically changed, according to eqs 13-14); see systematic discussions in ref.[95]

■ ANISOTROPIC META-BOUNDARY

One typical feature of anisotropic meta-boundaries is their distinct response to TE and TM waves. That is, the anisotropic meta-boundary is sensitive to the incident polarization of light and can be exploited to perform many polarization-based functions, including polarization selectivity, polarization conversion, and perfect absorption of light with specific absorption.[69,96−104] For example, the application of anisotropic meta-boundaries can result in the spatial separation of light with different linear polarizations.[98] Utilizing single or multiple vertically parallel anisotropic meta-boundaries can realize the conversion between the circularly polarized light (Figure 3a) and linearly polarized light.[104] If the anisotropic meta-boundary has certain nonlinear effect, the laser-mode locking can be achieved; that is, only the laser mode with a specific polarization at the prescribed frequency can be retained in Figure 3b.[105] Figure 3c shows that the anisotropic meta-boundary plays an important role in spatially molding the propagation of surface waves.[106]

Among various anisotropic meta-boundaries, the hyperbolic meta-boundary is of particular interest, whose corresponding electric and/or magnetic surface conductivities have $\sigma_{e,xx}\cdot\sigma_{e,yy} < 0$ and $\sigma_{m,xx}\cdot\sigma_{m,yy} < 0$, where $\overline{\overline{\sigma}}_e = \mathrm{diag}\,[\sigma_{e,xx}\ \sigma_{e,yy}]$ and $\overline{\overline{\sigma}}_m = \mathrm{diag}\,[\sigma_{m,xx}\ \sigma_{m,yy}]$. One key advantage of hyperbolic meta-boundaries is their capability to support hyperbolic plasmons (see their near-field excitation in Figure 3d, for example), whose

https://doi.org/10.1021/acsphotonics.2c01705
ACS Photonics XXXX, XXX, XXX−XXX

isofrequency contour is hyperbolic.[106−112] Due to the highly squeezed nature of hyperbolic plasmons in space, hyperbolic meta-boundaries have been extensively used to manipulate the flow of nanolight, especially for the realization of propagation with high directionality. Therefore, the hyperbolic meta-boundaries enable a variety of optical functions at the deep-subwavelength scale, such as plasmonic superlens, enhanced spontaneous emission, and directional guidance at the nanoscale.[113−121] On the other hand, low-dimensional materials provide an abundant choice for the construction of hyperbolic meta-boundaries.[122−125] For example, hyperbolic meta-boundaries can be fabricated by patterning isotropic low-dimensional materials (e.g., nanoribbons arrays of graphene or hexagonal boron nitride (BN) in Figure 3d,e or by using naturally anisotropic materials (e.g., doped monolayer black phosphorus in Figure 3f).[46,110,126]

BIISOTROPIC META-BOUNDARY

Distinct from the isotropic and anisotropic meta-boundaries, the biisotropic meta-boundary has magnetoelectric coupling,[127−136] which is modeled by the magnetoelectric surface conductivities in eqs 17 and 18. In order to introduce the magnetoelectric coupling, the electromagnetic boundary becomes relatively complex in the structural fabrication and should be carefully designed. The realization of biisotropic meta-boundaries may require, for example, the usage of single metasurface with some irregular bulges in Figure 4a or the vertical stacking of multiple metasurfaces with a special interlayer twisted angle in Figure 4b.[130,131] Moreover, to ensure the isotropy of magnetoelectric coupling, these metasurfaces should have a good rotational symmetry. Figure 3c shows that the time-modulated metasurface, which consists of metallic patches array and parallel capacitor, may provide another route for the design of biisotropic meta-boundary.[132] Meanwhile, the biisotropic boundary can be achieved by inserting chiral materials (which intrinsically have the isotropic magnetoelectric coupling) into an ultrathin dielectric slab in Figure 3d.[133] With the help of the biisotropic meta-boundary, the scattering cross section of certain objects can be reduced significantly.[135] If the biisotropic meta-boundary is spatiotemporally modulated, one may further realize the nonreciprocal transmission of light.[132]

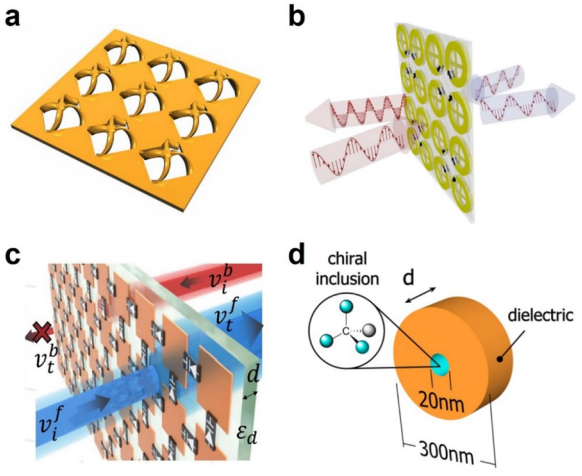

Figure 4. Biisotropic meta-boundaries. (a) Pinwheel-like metasurface; reprinted with permission from ref 130. Copyright 2018 AAAS. (b) Bilayer biisotropic metasurface; reprinted with permission from ref 131. Copyright 2016 American Physical Society. (c) Time-modulated metasurface comprised of metallic patches array and parallel capacitors; reprinted with permission from ref 132. Copyright 2020 American Physical Society. (d) Chiral metasurfaces with their unit cell constructed by a dielectric nanodisk and a chiral inclusion; reprinted with permission from ref 133. Copyright 2020 American Physical Society.

Despite these recent advances, the fabrication of biisotropic meta-boundaries still lacks a systematic methodology and remains a challenge. Accordingly, the biisotropic meta-boundary has been rarely explored when compared with the isotropic and anisotropic ones.

BIANISOTROPIC META-BOUNDARY

For bianisotropic meta-boundaries, their fabrication[137−139] can be relatively easier when compared with biisotropic meta-boundariers, since there is no need to keep the isotropy of magnetoelectric coupling. For instance, the metasurface with the Omega-type meta-atom, which has strong anisotropic magnetoelectric coupling and is relatively simple in fabrication in Figure 5a,[140,141] provides a typical route to construct the bianisotropic meta-boundary. Apart from metal-based metasurfaces, the bianisotropic meta-boundary can also be designed by arrays of all-dielectric cylindrical rods with an irregular hole. Figure 5b shows that this kind of bianisotropic meta-boundary can have a large nonlinear effect, which can induce a giant asymmetric second harmonic generation.[137] While bianisotropic metasurfaces provide a versatile platform for the construction of bianisotorpic meta-boundaries, the calculation or retrieval of their effective surface conductivity is generally very complicated. Despite the complexity, the relevant calculation or retrieval has been extensively investigated[142−144] and is, in principle, feasible, for example, by applying the homogenization model based polarizabilities.[145,146] One advantage of this model is that it offers a straightforward route to determine what kind of constituents that should be incorporated into the metasurface in order to obtain the desired optical response of metasurface.[142,146] Another advantage of this model allows the rigorous engineering of the whole metasurface through the calculation of the required polarizabilities of individual inclusions, if each inclusion sits in free space and does not interact with other inclusions.[146] Moreover, recent works show that the twisted bilayer graphene in Figure 5c can facilitate the design of novel bianisotropic meta-boundaries, since the twisted bilayer graphene intrinsically possesses the bianisotropy, which originates from the interlayer quantum coupling.[147−153] Moreover, the bianisotropic meta-boundary assisted by the twisted bilayer graphene can support the propagation of chiral plasmons, which have not only the transverse spin but also the longitudinal spin.[150] This way, new kinds of spin−orbit interaction of light are expected in these bianisotropic meta-boundaries but await further exploration both in theory and experiments.

Despite the complexity of their electromagnetic boundary conditions in eqs 19 and 20, bianisotropic meta-boundaries have demonstrated unique applications in the manipulation of light−matter interactions. For example, bianisotropic meta-boundaries are capable to realize the complete polarization conversion during either the reflection or transmission process in Figure 5d.[149,154] With the help of bianisotropic meta-boundaries, the polarization of free-electron radiation (e.g., Smith-Purcell radiation in Figure 5e) can be arbitrarily designed.[45,155−157] In addition, the bianisotropic meta-

https://doi.org/10.1021/acsphotonics.2c01705
ACS Photonics XXXX, XXX, XXX−XXX

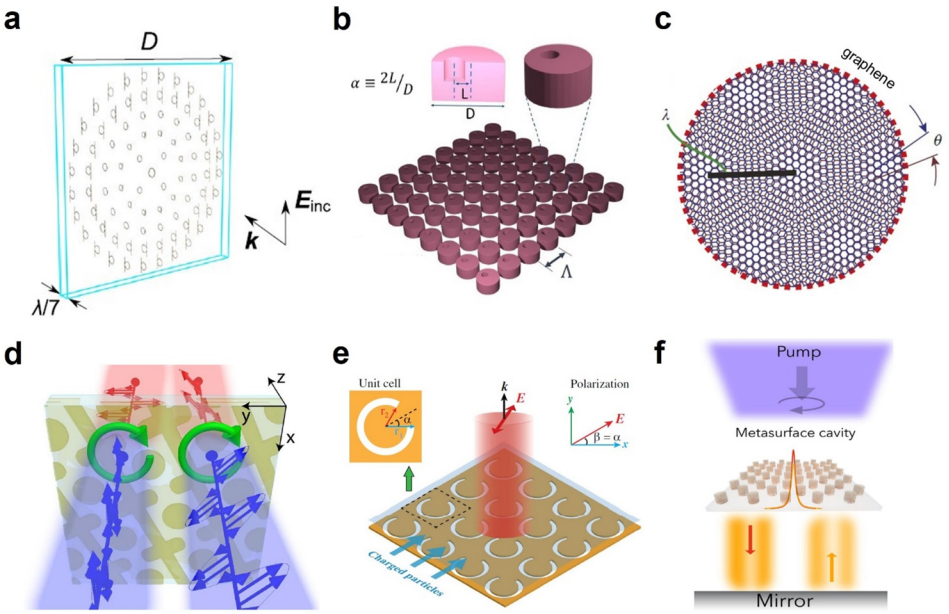

Figure 5. Bianisotropic meta-boundaries. (a) Functional meta-mirrors using bianisotropic elements; reprinted with permission from ref 140. Copyright 2015 American Physical Society. (b) All-dielectric bianisotrapic metasurface; reprinted with permission from ref 137. Copyright 2021 American Chemical Society. (c) Twisted bilayer graphene; reprinted with permission from ref 147. Copyright 2018 Springer Nature. (d) Polarization rotation with ultrathin bianisotropic metasurfaces; reprinted with permission from ref 154. Copyright 2016 Optica. (e) Smith-Purcell radiation from bianisotropic metasurfaces; reprinted with permission from ref 45. Copyright 2016 American Physical Society. (f) Self-isolated Raman lasing with a chiral dielectric metasurface; reprinted with permission from ref 158. Copyright 2021 American Physical Society.

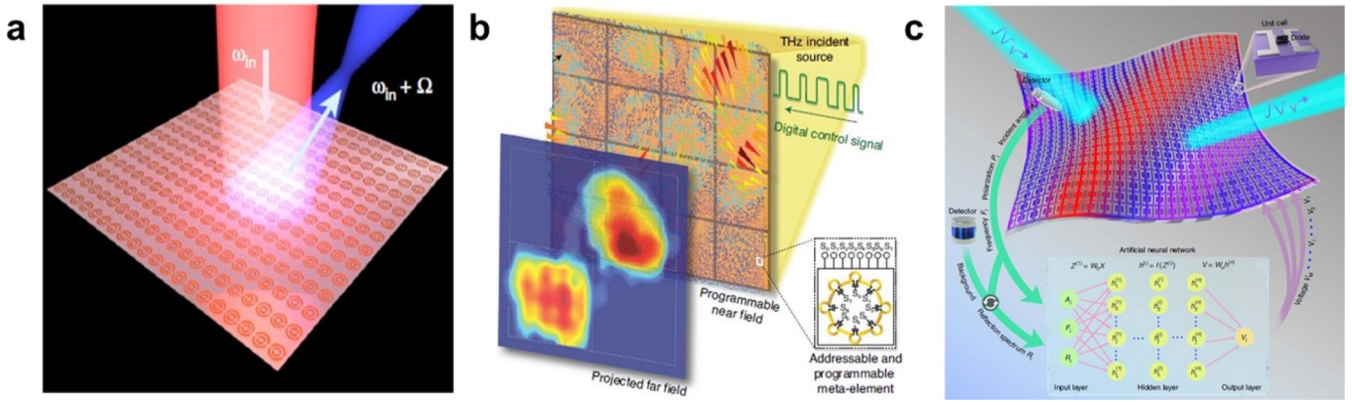

Figure 6. Active meta-boundaries. (a) Spatiotemporal metasurfaces, which can tune the frequency of reflected light and converge the reflected light at a predesigned focal point; reprinted with permission from ref 166. Copyright 2020 Springer Nature. Distributed under a CC BY 4.0 license https://creativecommons.org/licenses/by/4.0/. (b) Dynamically programmable metasurfaces, which is made of a programmable two-dimensional array of meta-elements; reprinted with permission from ref 172. Copyright 2020 Springer Nature. (c) Self-adaptive metasurface cloak enabled by deep learning; reprinted with permission from ref 178. Copyright 2020 Springer Nature.

boundary is widely used in other realms, including the transformation of propagating waves into surface waves, self-isolated Raman lasing in Figure 5f, and asymmetric transmission of light.[158,159]

■ ACTIVE META-BOUNDARY

One rising tendency for the further exploration of meta-boundary is the investigation of active (or temporal) meta-boundary, which is temporally modulated and thus whose corresponding surface conductivity is a function of time. Due to the existence of time modulation, the active meta-boundaries can be exploited to realize exotic performance, including the dynamical beam steering, nonreciprocal transmission of light, real-time on-chip communications, and Doppler-like frequency shift of light.[160−170] Figure 6a shows that the active meta-boundary can tune the frequency of reflected light and converge the reflected light into any predesigned focal point.[166]

To further improve the capability of meta-boundaries, one may add the spatial modulation into the active meta-boundary. Such kinds of active (or spatiotemporal) meta-boundaries can be achieved by actively and separately tuning each unit cell of metasurface, through the electronic or optical programming.[171−177] These active meta-boundaries can perform many advanced functions, such as intelligent communication and holographic imaging. Figure 6b shows one typical active meta-boundary, which is created by arrays of complementary metal-oxide-semiconductor (CMOS)-based chip tiles and can digitally control the amplitude and phase of light.[172] These

https://doi.org/10.1021/acsphotonics.2c01705
ACS Photonics XXXX, XXX, XXX−XXX

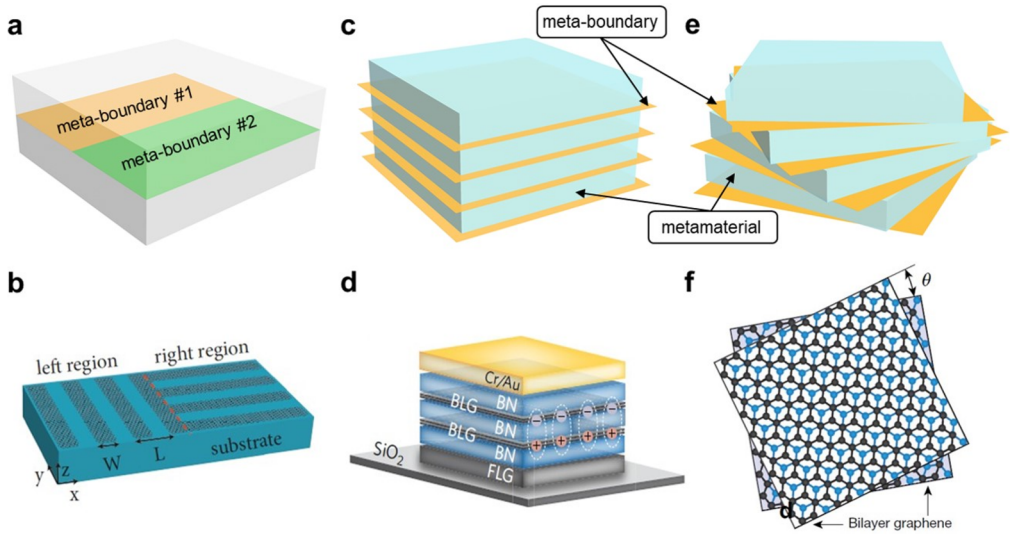

Figure 7. Multilayer meta-boundaries. (a) Schematic of horizontally stacking multiple meta-boundaries in a same plane. (b) Example of (a), such as the creation of a line boundary by using two hyperbolic metasurfaces with different in-plane rotations; reprinted with permission from ref 186. Copyright 2018 AAAS. (c) Schematic of vertically stacking meta-boundaries in multiple parallel planes without interlayer twisted angles. (d) Example of (c), such as the construction of multilayer heterostructures by using bilayer graphene and the hyperbolic slab (e.g., hexagonal BN); reprinted with permission from ref 187. Copyright 2017 Springer Nature. (e) Schematic of vertically stacking meta-boundaries in multiple parallel planes with interlayer twisted angles. (f) Example of (e), such as the twisted double bilayer graphene; reprinted with permission from ref 199. Copyright 2020 Springer Nature.

active meta-boundaries are then advantageous in controlling the scattering of light in real time. For example, Figure 6c shows that the real-time self-adaptive cloak can be implemented based on the active meta-boundary with the aid of artificial intelligence.[178] To be specific, though inserting an artificial neural network between the detection system and the control system, the active meta-boundary behaves as a carpet cloak with a very small scattering cross section, regardless of the real-time change of surrounding environment.

MULTIPLE META-BOUNDARIES

Apart from individual meta-boundary, multiple meta-boundaries can be combined, which may induce the in-plane or out-of-plane interactions between neighboring meta-boundaries. Due to the rich yet relatively less explored physics in these in-plane and out-of-plane interactions, the exploration of multiple meta-boundaries is becoming another research tendency.[179−185]

To induce the in-plane interaction, one way is to splice two different meta-boundaries in a same plane, as schematically shown in Figure 7a. As a result, the in-plane splicing between two meta-boundaries can give rise to a high-order boundary, namely, a one-dimensional line interface. Correspondingly, the existence of high-order boundary can induce the phenomena of reflection, transmission and even scattering for surface waves. For example, Figure 7b shows the in-plane splicing between two hyperbolic meta-boundaries, which are the same but have different orientation angles. Remarkably, the appearance of high-order boundary between these two hyperbolic meta-boundaries can support the phenomenon of all-angle negative refraction of highly squeezed hyperbolic plasmons within a broad frequency regime.[186] On the other hand, it is worthy to note that during the reflection and transmission process of surface waves, the scattering of surface waves into propagating waves generally exists, which indicates an unwanted degradation of signals and may induce a noisy electromagnetic background. Therefore, the suppression of this scattering has been long sought after but is still challenging in experiments. The realization of this enticing goal based on the high-order boundary in Figure 7a, which is formed by diverse meta-boundaries, might be promising but remains unexplored.

To induce the out-of-plane interaction between meta-boundaries, one way is to vertically stack multiple parallel but spatially separated meta-boundaries, as shown in Figure 7c. For example, Figure 7d shows the schematic structure of double bilayer graphene, separated by thin BN slabs. Remarkably, this kind of multiple meta-boundaries can support the emergence of excitonic superfluid phase.[187] Moreover, the out-of-plane interaction between neighboring meta-boundaries would become more complex, if there exists the interlayer twist angle,[188−198] as schematically shown in Figure 7e. For example, Figure 7f shows the multiple meta-boundaries composed of rotated multiple bilayer graphene.[199] The canalized excitation and propagation of surface waves can be achieved by stacking multiple α-phase molybdenum trioxide (α-MoO_3) slabs, in which an ultrathin slab of α-MoO_3 may be approximately modeled by an anisotropic metasurface.[189] Moreover, the phenomenon of topological transition for the iso-frequency contour of surface waves would occur, readily by rotating the interlayer twist angle.

COMPOSITE STRUCTURES COMPOSED OF META-BOUNDARIES AND METAMATERIALS

Meta-boundaries have shown impressive capabilities to tailor the optical response of the interface, while metamaterials have shown impressive capabilities to tailor the optical response of bulk media. Therefore, it is straightforward to combine meta-boundaries and metamaterials in a same structure (see the schematic in Figure 8a). Since both meta-boundaries and metamaterials can be isotropic, anisotropic, biisotropic and bianisotropic, there are various possible combinations between them;[200−204] see the brief schematic summarization in Figure 8b. Then the composite structures, which simultaneously have

https://doi.org/10.1021/acsphotonics.2c01705
ACS Photonics XXXX, XXX, XXX−XXX

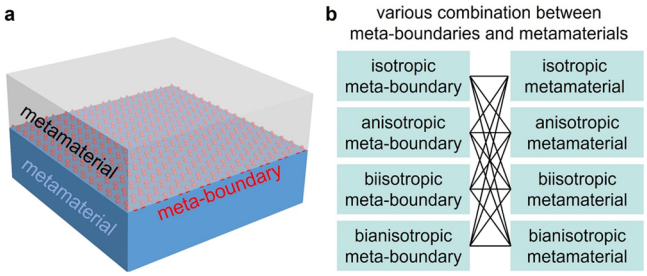

Figure 8. Controlling light−matter interactions by exploiting meta-boundaries and metamaterials. (a) Structural illustration of a meta-boundary covered and supported by metamaterials. (b) Various combination between meta-boundaries and metamaterials. The left blocks represent various meta-boundaries. The right blocks represent various metamaterials. Each solid line that links the left block and the right block indicates the possible combination between one specific meta-boundary and one specific metamaterial.

meta-boundaries and metamaterials, are promising to provide a powerful yet plentiful platform for the manipulation of light−matter interactions. Therefore, these composite structures are worthy of more in-depth and systematic exploration.

For example, Figure 9a,b shows two composite structures by depositing a two-dimensional transition metal dichalcogenides (TMD) material on a grating or a two-dimensional photonic crystal,[200,201] both of which can be treated as a metamaterial with strong nonlocality. These composite structures can flexibly tailor the topological property of polaritonic systems. Figure 9c shows another composite structure by placing a monolayer graphene on a uniaxial BN slab with a finite thickness. This composite structure is able to realize the all-angle negative refraction of highly squeezed isotropic surface waves.[11] Figure 9d further shows that the composite structure composed of the monolayer graphene and an α-MoO_3 slab can facilitate the realization of polaritonic focus.[196]

In conclusion, we have highlighted the importance of meta-boundaries in controlling the light-matter interactions. After reviewing the recent progresses on isotropic, anisotropic, biiostropic and bianisotropic meta-boundaries, the research tendencies for meta-boundaries are analyzed, including the continuing exploration of active meta-boundaries, multiple meta-boundaries, and composite structures composed of meta-boundaries and metamaterials. Regarding composite structures, most current researches are mainly carried out for relatively simple composite structures, which are composed of isotropic or anisotropic meta-boundaries and isotropic or anisotropic metamaterials. The relatively complex composite structure, such as those composed of bianisotropic meta-boundaries and bianisotropic metamaterials, demands more extensive and in-depth studies.

AUTHOR INFORMATION

Corresponding Authors

Xiao Lin − *Interdisciplinary Center for Quantum Information, State Key Laboratory of Modern Optical Instrumentation, ZJU-Hangzhou Global Scientific and Technological Innovation Center, Zhejiang University, Hangzhou 310027, China; International Joint Innovation Center, Key Lab. of Advanced Micro/Nano Electronic Devices & Smart Systems of Zhejiang, The Electromagnetics Academy at Zhejiang University, Zhejiang University, Haining 314400, China*; Email: xiaolinzju@zju.edu.cn

Tong Cai − *Interdisciplinary Center for Quantum Information, State Key Laboratory of Modern Optical Instrumentation, ZJU-Hangzhou Global Scientific and Technological Innovation Center, Zhejiang University, Hangzhou 310027, China; Air and Missile Defense College,*

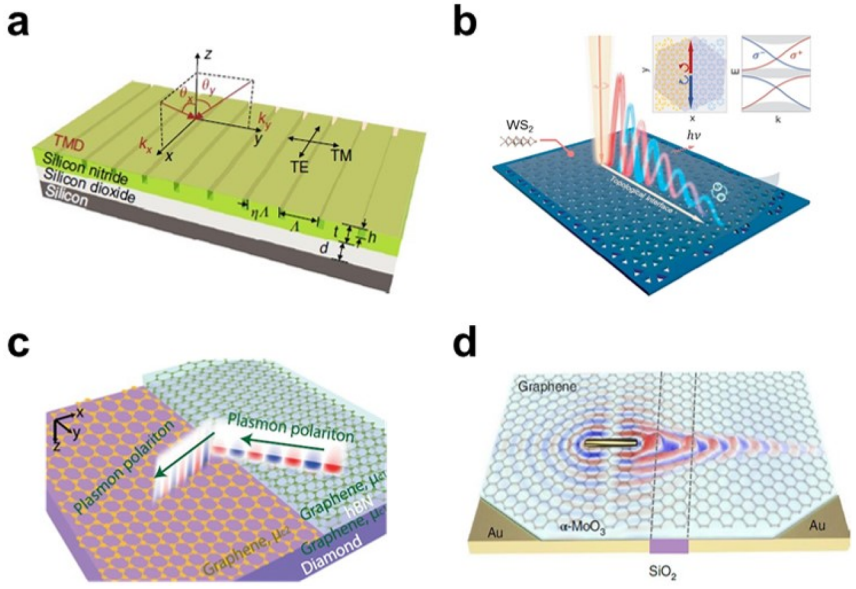

Figure 9. Examples of controlling light−matter interactions by using meta-boundaries and metamaterials. (a) Generation of exciton-polaritons in monolayer transition metal dichalcogenides (TMD), which is supported by a grating made of silicon nitride; reprinted with permission from ref 200. Copyright 2020 Springer Nature. (b) Generation of helical topological exciton−polaritons in tungsten disulfide (WS_2), which is supported by a two-dimensional photonic crystal; reprinted with permission from ref 201. Copyright 2020 AAAS. (c) Negative refraction of highly squeezed polaritons in a graphene-hexagonal boron nitride (BN) heterostructure; reprinted with permission from ref 11. Copyright 2017 National Academy of Science. (d) Polaritonic focusing in a graphene/α-phase molybdenum trioxide (α-MoO_3) heterostructure; reprinted with permission from ref 196. Copyright 2022 Springer Nature.

https://doi.org/10.1021/acsphotonics.2c01705
ACS Photonics XXXX, XXX, XXX−XXX

Air Force Engineering University, Xi' an 710051, China; Email: caitong326@zju.edu.cn

Hongsheng Chen − *Interdisciplinary Center for Quantum Information, State Key Laboratory of Modern Optical Instrumentation, ZJU-Hangzhou Global Scientific and Technological Innovation Center, Zhejiang University, Hangzhou 310027, China; International Joint Innovation Center, Key Lab. of Advanced Micro/Nano Electronic Devices & Smart Systems of Zhejiang, The Electromagnetics Academy at Zhejiang University, Zhejiang University, Haining 314400, China*; orcid.org/0000-0002-5735-9781; Email: hansomchen@zju.edu.cn

Authors

Xinyan Zhang − *Interdisciplinary Center for Quantum Information, State Key Laboratory of Modern Optical Instrumentation, ZJU-Hangzhou Global Scientific and Technological Innovation Center, Zhejiang University, Hangzhou 310027, China; International Joint Innovation Center, Key Lab. of Advanced Micro/Nano Electronic Devices & Smart Systems of Zhejiang, The Electromagnetics Academy at Zhejiang University, Zhejiang University, Haining 314400, China*

Jialin Chen − *Interdisciplinary Center for Quantum Information, State Key Laboratory of Modern Optical Instrumentation, ZJU-Hangzhou Global Scientific and Technological Innovation Center, Zhejiang University, Hangzhou 310027, China; International Joint Innovation Center, Key Lab. of Advanced Micro/Nano Electronic Devices & Smart Systems of Zhejiang, The Electromagnetics Academy at Zhejiang University, Zhejiang University, Haining 314400, China*

Ruoxi Chen − *Interdisciplinary Center for Quantum Information, State Key Laboratory of Modern Optical Instrumentation, ZJU-Hangzhou Global Scientific and Technological Innovation Center, Zhejiang University, Hangzhou 310027, China; International Joint Innovation Center, Key Lab. of Advanced Micro/Nano Electronic Devices & Smart Systems of Zhejiang, The Electromagnetics Academy at Zhejiang University, Zhejiang University, Haining 314400, China*

Chan Wang − *Interdisciplinary Center for Quantum Information, State Key Laboratory of Modern Optical Instrumentation, ZJU-Hangzhou Global Scientific and Technological Innovation Center, Zhejiang University, Hangzhou 310027, China; International Joint Innovation Center, Key Lab. of Advanced Micro/Nano Electronic Devices & Smart Systems of Zhejiang, The Electromagnetics Academy at Zhejiang University, Zhejiang University, Haining 314400, China*

Reza Abdi-Ghaleh − *Deparment of Laser and Optical Engineering, University of Bonab, Bonab 5551395133, Iran*

Complete contact information is available at: https://pubs.acs.org/10.1021/acsphotonics.2c01705

Funding

The National Natural Science Foundation of China (NSFC); the National Natural Science Fund for Excellent Young Scientists Fund Program (Overseas) of China; the Fundamental Research Funds for the Central Universities (2021FZZX001-19); Zhejiang University Global Partnership Fund; the Key Research and Development Program of the Ministry of Science and Technology; the Chinese Scholarship Council (CSC No. 202206320287).

Notes

The authors declare no competing financial interest.

■ ACKNOWLEDGMENTS

The work at Zhejiang University was sponsored in part by the National Natural Science Foundation of China (NSFC) under Grants No. 62175212, the National Natural Science Fund for Excellent Young Scientists Fund Program (Overseas) of China, the Fundamental Research Funds for the Central Universities (2021FZZX001-19), Zhejiang University Global Partnership Fund, the Key Research and Development Program of the Ministry of Science and Technology under Grants No. 2022YFA1404704, 2022YFA1404902, and SQ2022YFA1400025, the National Natural Science Foundation of China (NNSFC) under Grant Nos.11961141010 and 61975176, the Fundamental Research Funds for the Central Universities, and the Chinese Scholarship Council (CSC No. 202206320287).

■ REFERENCES

(1) Ee, H. S.; Agarwal, R. Tunable metasurface and flat optical zoom lens on a stretchable substrate. *Nano Lett.* **2016**, *16*, 2818−2823.

(2) Zheng, G.; Muhlenbernd, H.; Kenney, M.; Li, G.; Zentgraf, T.; Zhang, S. Metasurface holograms reaching 80% efficiency. *Nat. Nanotechnol.* **2015**, *10*, 308−312.

(3) Xie, Y.; Wang, W.; Chen, H.; Konneker, A.; Popa, B.-I.; Cummer, S. A. Wavefront modulation and subwavelength diffractive acoustics with an acoustic metasurface. *Nat. Commun.* **2014**, *5*, 5553.

(4) Huang, L.; Chen, X.; Muhlenbernd, H.; Zhang, H.; Chen, S.; Bai, B.; Tan, Q.; Jin, G.; Cheah, K.-W.; Qiu, C.-W.; Li, J.; Zentgraf, T.; Zhang, S. Three-dimensional optical holography using a plasmonic metasurface. *Nat. Commun.* **2013**, *4*, 2808.

(5) Pors, A.; Nielsen, M. G.; Eriksen, R. L.; Bozhevolnyi, S. I. Broadband focusing flat mirrors based on plasmonic gradient metasurfaces. *Nano Lett.* **2013**, *13*, 829−834.

(6) Fetter, A. L. Electrodynamics and thermodynamics of a classical electron surface layer. *Phys. Rev. B* **1974**, *10*, 3739−3745.

(7) Stern, F. Polarizability of a two-dimensional electron gas. *Phys. Rev. Lett.* **1967**, *18*, 546−548.

(8) Cai, T.; Tang, S.; Zheng, B.; Wang, G.; Ji, W.; Qian, C.; Wang, Z.; Li, E.; Chen, H. Ultrawideband chromatic aberration-free metamirrors. *Adv. Photon.* **2021**, *3*, No. 016001.

(9) Overviga, A.; Alù, A. Wavefront-selective Fano resonant metasurfaces. *Adv. Photon.* **2021**, *3*, No. 026002.

(10) Qian, C.; Yang, Y.; Hua, Y.; Wang, C.; Lin, X.; Cai, T.; Ye, D.; Li, E.; Kaminer, I.; Chen, H. Breaking the fundamental scattering limit with gain metasurfaces. *Nat. Common.* **2022**, *13*, 4383.

(11) Lin, X.; Yang, Y.; Rivera, N.; López, J. J.; Shen, Y.; Kaminer, I.; Chen, H.; Zhang, B.; Joannopoulos, J. D.; Soljačić, M. All-angle negative refraction of highly squeezed plasmon and phonon polaritons in graphene-boron nitride heterostructures. *Proc. Natl. Acad. Sci. U.S.A.* **2017**, *114*, 6717−6721.

(12) Verhagen, E.; de Waele, R.; Kuipers, L.; Polman, A. Three-dimensional negative index of refraction at optical frequencies by coupling plasmonic waveguides. *Phys. Rev. Lett.* **2010**, *105*, 223901.

(13) Zhang, S.; Park, Y.-S.; Li, J.; Lu, X.; Zhang, W.; Zhang, X. Negative refractive index in chiral metamaterials. *Phys. Rev. Lett.* **2009**, *102*, No. 023901.

(14) Valentine, J.; Zhang, S.; Zentgraf, T.; Ulin-Avila, E.; Genov, D. A.; Bartal, G.; Zhang, X. Three-dimensional optical metamaterial with a negative refractive index. *Nature* **2008**, *455*, 376−380.

(15) Smith, D. R.; Padilla, W. J.; Vier, D. C.; Nemat-Nasser, S. C.; Schultz, S. Composite medium with simultaneously negative permeability and permittivity. *Phys. Rev. Lett.* **2000**, *84*, 4184−4187.

(16) Cubukcu, E.; Aydin, K.; Ozbay, E.; Foteinopoulou, S.; Soukoulis, C. M. Electromagnetic waves: negative refraction by photonic crystals. *Nature* **2003**, *423*, 604−605.
(17) Zhao, M.; et al. Phase characterisation of metalenses. *Light Sci. Appl.* **2021**, *10*, 52.
(18) Yang, W.; Xiao, S.; Song, Q.; Liu, Y.; Wu, Y.; Wang, S.; Yu, J.; Han, J.; Tsai, D.-P. All-dielectric metasurface for high-performance structural color. *Nat. Commun.* **2020**, *11*, 1−8.
(19) Chen, H.; Wu, B.-I.; Zhang, B.; Kong, J. A. Electromagnetic wave interactions with a metamaterial cloak. *Phys. Rev. Lett.* **2007**, *99*, No. 063903.
(20) Cai, T.; Zheng, B.; Lou, J.; Shen, L.; Yang, Y.; Tang, S.; Li, E.; Qian, C.; Chen, H. Experimental realization of a superdispersion-enabled ultrabroadband terahertz cloak. *Adv. Mater.* **2022**, *34*, 2205053.
(21) Xu, S.; Xu, H.; Gao, H.; Jiang, Y.; Yu, F.; Joannopoulos, J.; Soljacic, M.; Chen, H.; Sun, H.; Zhang, B. Broadband surface-wave transformation cloak. *Proc. Natl. Acad. Sci. U.S.A.* **2015**, *112*, 7635−7638.
(22) Chen, H.; Zheng, B.; Shen, L.; Wang, H.; Zhang, X.; Zheludev, N. I.; Zhang, B. Ray-optics cloaking devices for large objects in incoherent natural light. *Nat. commun.* **2013**, *4*, 2652.
(23) Pendry, J. B.; Schurig, D.; Smith, D. R. Controlling electromagnetic fields. *Science* **2006**, *312*, 1780−1782.
(24) Leonhardt, U. Optical conformal mapping. *Science* **2006**, *312*, 1777−1780.
(25) Lindell, I. V.; Sihvola, A. Generalization of perfect electromagnetic conductor boundary. *IEEE Trans. Antennas Propag.* **2020**, *68*, 7406−7413.
(26) Lindell, I. V.; Sihvola, A. Generalized soft-and-hard/DB boundary. *IEEE Trans. Antennas Propag.* **2017**, *65*, 226−233.
(27) Gutzler, R.; Garg, M.; Ast, C. R.; Kuhnke, K.; Kern, K. Light-matter interaction at atomic scales. *Nat. Rev. Phys.* **2021**, *3*, 441−453.
(28) Rivera, N.; Kaminer, I. Light-matter interactions with photonic quasiparticles. *Nat. Rev. Phys.* **2020**, *2*, 538−561.
(29) Lu, X.; Shapiro, M. A.; Mastovsky, I.; Temkin, R. J.; Conde, M.; Power, J. G.; Shao, J.; Wisniewski, E. E.; Jing, C. Generation of high-power, reversed-Cherenkov wakefield radiation in a metamaterial structure. *Phys. Rev. Lett.* **2019**, *122*, No. 014801.
(30) Duan, Z.; Tang, X.; Wang, Z.; Zhang, Y.; Chen, X.; Chen, M.; Gong, Y. Observation of the reversed Cherenkov radiation. *Nat. Commun.* **2017**, *8*, 14901.
(31) Watts, C. M.; Liu, X.; Padilla, W. J. Metamaterial electromagnetic wave absorbers. *Adv. Mater.* **2012**, *24*, 98−120.
(32) Xi, S.; Chen, H.; Jiang, T.; Ran, L.; Huangfu, J.; Wu, B.-I.; Kong, J. A.; Chen, M. Experimental verification of reversed Cherenkov radiation in left-handed metamaterial. *Phys. Rev. Lett.* **2009**, *103*, 194801.
(33) Landy, N. I.; Sajuyigbe, S.; Mock, J. J.; Smith, D. R.; Padilla, W. J. Perfect metamaterial absorber. *Phys. Rev. Lett.* **2008**, *100*, 207402.
(34) Hu, H.; Lin, X.; Luo, Y. Free-electron radiation engineering via structured environments. *Prog. Electromagn. Res.* **2021**, *171*, 75−88.
(35) Chen, H.; Ran, L.; Huangfu, J.; Zhang, X.; Chen, K.; Grzegorczyk, T. M.; Au Kong, J. Left-handed materials composed of only S-shaped resonators. *Phys. Rev. E* **2004**, *70*, No. 057605.
(36) Soukoulis, C. M.; Wegener, M. Past achievements and future challenges in the development of three-dimensional photonic metamaterials. *Nat. Photonics* **2011**, *5*, 523−530.
(37) Gansel, J. K.; Thiel, M.; Rill, M. S.; Decker, M.; Bade, K.; Saile, V.; von Freymann, G.; Linden, S.; Wegener, M. Gold helix photonic metamaterial as broadband circular polarizer. *Science* **2009**, *325*, 1513−1515.
(38) Liu, N.; Fu, L. W.; Kaiser, S.; Schweizer, H.; Giessen, H. Plasmonic building blocks for magnetic molecules in three-dimensional optical metamaterials. *Adv. Mater.* **2008**, *20*, 3859−3865.
(39) Kawata, S.; Ono, A.; Verma, P. Subwavelength colour imaging with a metallic nanolens. *Nat. Photonics* **2008**, *2*, 438−442.
(40) Kong, J. A. *Electromagnetic Wave Theory*; EMW Publishing, 2008.
(41) Chen, X.; Li, M.; Chen, W.; Yang, H.; Pei, Z.; Li, E.; Chen, H.; Wang, Z. Broadband Janus scattering from tilted dipolar metagratings. *Laser Photonics Rev.* **2022**, *16*, 2100369.
(42) Wang, C.; Zhang, Z.; Zhang, Y.; Xie, X.; Yang, Y.; Han, J.; Li, E.; Chen, H.; Gu, J.; Sha, W. E I; Gao, F. Enhancing directivity of terahertz photoconductive antennas using spoof surface plasmon structure. *New J. Phys.* **2022**, *24*, No. 073046.
(43) Zhang, H.; Sun, J.; Yang, J.; De Leon, I.; Zaccaria, R. P.; Qian, H.; Chen, H.; Wang, G.; Wang, T. Biosensing performance of a plasmonic-grating-based nanolaser. *Prog. Electromagn. Res.* **2021**, *171*, 159−169.
(44) Li, Z.; Cao, G.; Li, C.; Dong, S.; Deng, Y.; Liu, X.; Ho, J. S.; Qiu, C.-W. Non-Hermitian electromagnetic metasurfaces at exceptional points. *Prog. Electromagn. Res.* **2021**, *171*, 1−20.
(45) Wang, Z.; Yao, K.; Chen, M.; Chen, H.; Liu, Y. Manipulating Smith-Purcell emission with Babinet metasurface. *Phys. Rev. Lett.* **2016**, *117*, 157401.
(46) Li, P.; Dolado, I.; Alfaro-Mozaz, F. J.; Casanova, F.; Hueso, L. E.; Liu, S.; Edgar, J. H.; Nikitin, A. Y.; Vélez, S.; Hillenbrand, R. Infrared hyperbolic metasurface based on nanostructured van der Waals materials. *Science* **2018**, *359*, 892−896.
(47) Basov, D. N.; Fogler, M. M.; García de Abajo, F. J. Polaritons in van der Waals materials. *Science* **2016**, *354*, 195−204.
(48) Mikhailov, S. A.; Ziegler, K. New electromagnetic mode in graphene. *Phys. Rev. Lett.* **2007**, *99*, No. 016803.
(49) Koppens, F. H. L.; Chang, D. E.; García de Abajo, F. J. Graphene plasmonics: A platform for strong light-matter interactions. *Nano Lett.* **2011**, *11*, 3370−3377.
(50) Geim, A. K.; Novoselov, K. S. The rise of graphene. *Nat. Mater.* **2007**, *6*, 183−191.
(51) Novoselov, K. S.; Geim, A. K.; Morozov, S. V.; Jiang, D.; Katsnelson, M. I.; Grigorieva, I. V.; Dubonos, S. V.; Firsov, A. A. Two dimensional gas of massless Dirac Fermions in graphene. *Nature* **2005**, *438*, 197−200.
(52) Geim, A. K.; Novoselov, K. S. The rise of graphene. *Nat. Mater.* **2007**, *6*, 183−191.
(53) Das Sarma, S.; Adam, S.; Hwang, E. H.; Rossi, E. Electronic transport in two-dimensional graphene. *Rev. Mod. Phys.* **2011**, *83*, 407−470.
(54) Sievenpiper, D.; Lijun Zhang; Broas, R.F.J.; Alexopolous, N.G.; Yablonovitch, E. High-impedance electromagnetic surface with a forbidden frequency band. IEEE. *Trans. Micro. Theory Technol.* **1999**, *47*, 2059−2074.
(55) Long, O. Y.; Guo, C.; Jin, W.; Fan, S. Polarization-independent isotropic nonlocal metasurfaces with wavelength-controlled functionality. *Phys. Rev. Appl.* **2022**, *17*, No. 024029.
(56) Zhang, C.; Divitt, S.; Fan, Q.; Zhu, W.; Agrawal, A.; Lu, Y.; Xu, T.; Lezec, H. J. Low-loss metasurface optics down to the deep ultraviolet region. *Light Sci. Appl.* **2020**, *9*, 55.
(57) Islam, M. S.; Sultana, J.; Biabanifard, M.; Vafapour, Z.; Nine, M. J.; Dinovitser, A.; Cordeiro, C. M. B.; Ng, B. W.-H.; Abbott, D. Tunable localized surface plasmon graphene metasurface for multi-band superabsorption and terahertz sensing. *Carbon* **2020**, *158*, 559−567.
(58) Chen, W. T.; Zhu, A. Y.; Capasso, F. Flat optics with dispersion-engineered metasurfaces. *Nat. Rev. Mater.* **2020**, *5*, 604−620.
(59) Fan, Y.; Shen, N.-H.; Zhang, F.; Zhao, Q.; Wu, H.; Fu, Q.; Wei, Z.; Li, H.; Soukoulis, C. M. Graphene plasmonics: a platform for 2D optics. *Adv. Optical Mater.* **2019**, *7*, 1800537.
(60) Li, Y. B.; Cai, B. G.; Cheng, Q.; Cui, T. J. Isotropic holographic metasurfaces for dual-functional radiations without mutual interferences. *Adv. Funct. Mater.* **2016**, *26*, 29−35.
(61) Huidobro, P. A.; Kraft, M.; Maier, S. A.; Pendry, J. B. Graphene as a tunable anisotropic or isotropic plasmonic metasurface. *ACS Nano* **2016**, *10*, 5499−5506.
(62) Sautter, J.; Staude, I.; Decker, M.; Rusak, E.; Neshev, Dr. N.; Brener, I.; Kivshar, Y. S. Active tuning of all-dielectric metasurfaces. *ACS Nano* **2015**, *9*, 4308−4315.

https://doi.org/10.1021/acsphotonics.2c01705
ACS Photonics XXXX, XXX, XXX−XXX

(63) Fei, Z.; et al. Gate-tuning of graphene plasmons revealed by infrared nano-imaging. *Nature* **2012**, *487*, 82−85.
(64) Padooru, Y. R.; Yakovlev, A. B.; Chen, P.-Y.; Alù, A. Analytical modeling of conformal mantle cloaks for cylindrical objects using sub-wavelength printed and slotted arrays. *J. Appl. Phys.* **2012**, *112*, No. 034907.
(65) Luukkonen, O.; Simovski, C.; Granet, G.; Goussetis, G.; Lioubtchenko, D.; Räisänen, A. V.; Tretyakov, S. A. Simple and accurate analytical model of planar grids and high-impedance surfaces comprising metal strips or patches. *IEEE Trans. Antennas Propag.* **2008**, *56*, 1624−1632.
(66) Divitt, S.; Zhu, W.; Zhang, C.; Lezec, H. J.; Agrawal, A. Ultrafast optical pulse shaping using dielectric metasurfaces. *Science* **2019**, *364*, 890−894.
(67) Kamali, S. M.; Arbabi, E.; Arbabi, A.; Faraon, A. A review of dielectric optical metasurfaces for wavefront control. *Nanophotonics* **2018**, *7*, 1041−1068.
(68) Arbabi, A.; Horie, Y.; Bagheri, M.; Faraon, A. Dielectric metasurfaces for complete control of phase and polarization with subwavelength spatial resolution and high transmission. *Nat. Nanotechnol.* **2015**, *10*, 937−943.
(69) Lin, D.; Fan, P.; Hasman, E.; Brongersma, M. L. Dielectric gradient metasurface optical elements. *Science* **2014**, *345*, 298−302.
(70) Low, T.; Roldán, R.; Wang, H.; Xia, F.; Avouris, P.; Moreno, L. M.; Guinea, F. Plasmons and screening in monolayer and multilayer black phosphorus. *Phys. Rev. Lett.* **2014**, *113*, 106802.
(71) Eguiluz, A.; Lee, T. K.; Quinn, J. J.; Chiu, K. W. Interface excitations in metal-insulator-semiconductor structures. *Phys. Rev. B* **1975**, *11*, 4989−4993.
(72) Sautter, J.; Staude, I.; Decker, M.; Rusak, E.; Neshev, Dr. N.; Brener, I.; Kivshar, Y. S. Active tuning of all-dielectric metasurfaces. *ACS Nano* **2015**, *9*, 4308−4315.
(73) Dai, S.; et al. Tunable phonon polaritons in atomically thin van der Waals crystals of boron nitride. *Science* **2014**, *343*, 1125−1129.
(74) Ponomarenko, L. A.; et al. Tunable metal-insulator transition in double-layer graphene heterostructures. *Nat. Phys.* **2011**, *7*, 958−961.
(75) Ci, L.; et al. Atomic layers of hybridized boron nitride and graphene domains. *Nat. Mater.* **2010**, *9*, 430−435.
(76) Zhang, Y.; Tang, T.-T.; Girit, C.; Hao, Z.; Martin, M. C.; Zettl, A.; Crommie, M. F.; Shen, Y. R.; Wang, F. Direct observation of a widely tunable bandgap in bilayer graphene. *Nature.* **2009**, *459*, 820−823.
(77) Shi, X.; Lin, X.; Kaminer, I.; Gao, F.; Yang, Z.; Joannopoulos, J. D.; Soljačić, M.; Zhang, B. Superlight inverse Doppler effect. *Nat. Phys.* **2018**, *14*, 1001−1005.
(78) Chen, J.; Chen, H.; Lin, X. Photonic and plasmonic transition radiation from graphene. *J. Opt.* **2021**, *23*, No. 034001.
(79) Smolyaninov, I. I. Surface electromagnetic waves at gradual interfaces between lossy media. *Prog. Electromagn. Res.* **2021**, *170*, 177−186.
(80) Pfeiffer, C.; Emani, N. K.; Shaltout, A. M.; Boltasseva, A.; Shalaev, V. M.; Grbic, A. Efficient light bending with isotropic metamaterial Huygens' surfaces. *Nano Lett.* **2014**, *14*, 2491−2497.
(81) Pfeiffer, C.; Grbic, A. Metamaterial Huygens' surfaces: tailoring wave fronts with reflectionless sheets. *Phys. Rev. Lett.* **2013**, *110*, 197401.
(82) Xie, H.; Hu, T.; Wang, Z.; Yang, Y.; Hu, X.; Qi, W.; Liu, H. A physics-based HIE-FDTD method for electromagnetic modeling of multi-band frequency selective surface. *Prog. Electromagn. Res.* **2022**, *173*, 129−140.
(83) Li, M.; Behdad, N. Frequency selective surfaces for pulsed high-power microwave applications. *IEEE Trans. Antennas Propag.* **2013**, *61*, 677−687.
(84) Sarabandi, K.; Behdad, N. A frequency selective surface with miniaturized elements. *IEEE Trans. Antennas Propag.* **2007**, *55*, 1239−1245.
(85) Lin, X.; Shen, Y.; Kaminer, I.; Chen, H. S.; Soljačić, M. Transverse-electric Brewster effect enabled by nonmagnetic two-dimensional materials. *Phys. Rev. A* **2016**, *94*, No. 023836.
(86) Alù, A.; D'Aguanno, G.; Mattiucci, N.; Bloemer, M. J. Plasmonic Brewster angle: broadband extraordinary transmission through optical gratings. *Phys. Rev. Lett.* **2011**, *106*, 123902.
(87) Paniagua-Domínguez, R.; et al. Generalized Brewster effect in dielectric metasurfaces. *Nat. Commun.* **2016**, *7*, 10362.
(88) Lin, X.; et al. A Brewster route to Cherenkov detectors. *Nat. Commun.* **2021**, *12*, 5554.
(89) Kim, S. Y.; Vedam, K. Analytic solution of the pseudo-Brewster angle. *J. Opt. Soc. Am. A* **1986**, *3*, 1772−1773.
(90) Shen, Y.; Ye, D.; Celanovic, I.; Johnson, S. G.; Joannopoulos, J. D.; Soljačić, M. Optical broadband angular selectivity. *Science* **2014**, *343*, 1499−1501.
(91) Grigorenko, A. N.; Polini, M.; Novoselov, K. S. Graphene plasmonics. *Nat. Photonics* **2012**, *6*, 749−758.
(92) Wong, J. L.; Kaminer, I.; Ilic, O.; Joannopoulos, J. D.; Soljačić, M. Towards graphene plasmon-based free-electron infrared to X-ray sources. *Nat. Photonics* **2016**, *10*, 46−52.
(93) Liu, L.; Han, Z.; He, S. Novel surface plasmon waveguide for high integration. *Opt. Express* **2005**, *13*, 6645−6650.
(94) Vakil, A.; Engheta, N. Transformation optics using graphene. *Science* **2011**, *332*, 1291−1294.
(95) Zhang, X.; Hu, H.; Lin, X.; Shen, L.; Zhang, B.; Chen, H. Confined transverse-electric graphene plasmons in negative refractive-index systems. *npj 2D Mater. Appl.* **2020**, *4*, 25.
(96) Balthasar Mueller, J. P.; Rubin, N. A.; Devlin, R. C.; Groever, B.; Capasso, F. Metasurface polarization optics: independent phase control of arbitrary orthogonal states of polarization. *Phys. Rev. Lett.* **2017**, *118*, 113901.
(97) Yang, Y.; Wang, W.; Moitra, P.; Kravchenko, I. I.; Briggs, D. P.; Valentine, J. Dielectric meta-reflectarray for broadband linear polarization conversion and optical vortex generation. *Nano Lett.* **2014**, *14*, 1394−1399.
(98) Ahn, S.-W.; Lee, K.-D.; Kim, J.-S.; Kim, S. H.; Park, J.-D.; Lee, S.-H.; Yoon, P.-W. Fabrication of a 50 nm half-pitch wire grid polarizer using nanoimprint lithography. *Nanotechnology* **2005**, *16*, 1874−1877.
(99) Wu, J. W.; Wang, Z. X.; Zhang, L.; Cheng, Q.; Liu, S.; Zhang, S.; Song, J. M.; Cui, T. J. Anisotropic metasurface holography in 3-D space with high resolution and efficiency. *IEEE Trans. Antennas Propag.* **2021**, *69*, 302−316.
(100) Shrestha, S.; Wang, Y.; Overvig, A. C.; Lu, M.; Stein, A.; Negro, L. D.; Yu, N. Indium tin oxide broadband metasurface absorber. *ACS Photonics* **2018**, *5*, 3526−3533.
(101) Kim, M.; Wong, A. M. H.; Eleftheriades, G. V. Optical Huygens' metasurfaces with independent control of the magnitude and phase of the local reflection coefficients. *Phys. Rev. X* **2014**, *4*, No. 041042.
(102) Grady, N. K.; Heyes, J. E.; Chowdhury, D. R.; Zeng, Y.; Reiten, M. T.; Azad, A. K.; Taylor, A. J.; Dalvit, D. A. R.; Chen, H.-T. Terahertz metamaterials for linear polarization conversion and anomalous refraction. *Science* **2013**, *340*, 1304−1306.
(103) Han, T.; Wen, K.; Xie, Z.; Yue, X. An ultra-thin wideband reflection reduction metasurface based on polarization conversion. *Prog. Electromagn. Res.* **2022**, *173*, 1−8.
(104) Zhao, Y.; Alù, A. Tailoring the dispersion of plasmonic nanorods to realize broadband optical meta-waveplates. *Nano Lett.* **2013**, *13*, 1086−1091.
(105) Sain, B.; Zentgraf, T. Metasurfaces help lasers to mode-lock. *Light Sci. Appl.* **2020**, *9*, 67.
(106) Gomez-Diaz, J. S.; Alù, A. Flatland optics with hyperbolic metasurfaces. *ACS Photonics* **2016**, *3*, 2211−2224.
(107) Wu, X.; McEleney, C. A.; Shi, Z.; González-Jiménez, M.; Macedo, R. Asymmetric reflection induced in reciprocal hyperbolic materials. *ACS Photonics* **2022**, *9*, 2774−2782.
(108) Zheng, Z.; et al. A midinfrared biaxial hyperbolic van der Waals crystal. *Sci. Adv.* **2019**, *5*, eaav8690.
(109) Chang, Y.-C.; Liu, C.-H.; Liu, C.-H.; Zhang, S.; Marder, S. R.; Narimanov, E. E.; Zhong, Z.; Norris, T. B. Realization of mid-infrared graphene hyperbolic metamaterials. *Nat. Commun.* **2016**, *7*, 1−12.

https://doi.org/10.1021/acsphotonics.2c01705
ACS Photonics XXXX, XXX, XXX−XXX

(110) Gomez-Diaz, J. S.; Tymchenko, M.; Alù, A. Hyperbolic plasmons and topological transitions over uniaxial metasurfaces. *Phys. Rev. Lett.* **2015**, *114*, 233901.
(111) High, A. A.; Devlin, R. C.; Dibos, A.; Polking, M.; Wild, D. S.; Perczel, J.; De Leon, N. P.; Lukin, M. D.; Park, H. Visible-frequency hyperbolic metasurface. *Nature* **2015**, *522*, 192−196.
(112) Poddubny, A.; Iorsh, I.; Belov, P.; Kivshar, Y. Hyperbolic metamaterials. *Nat. Photonics* **2013**, *7*, 948−957.
(113) Yang, Y.; Qin, P.; Lin, X.; Li, E.; Wang, Z.; Zhang, B.; Chen, H. Type-I hyperbolic metasurfaces for highly-squeezed designer polaritons with negative group velocity. *Nat. Commun.* **2019**, *10*, 2002.
(114) Galfsky, T.; Sun, Z.; Considine, C. R.; Chou, C.-T.; Ko, W.-C.; Lee, Y.-H.; Narimanov, E. E.; Menon, V. M. Broadband enhancement of spontaneous emission in two-dimensional semiconductors using photonic hypercrystals. *Nano Lett.* **2016**, *16*, 4940−4945.
(115) Caldwell, J. D.; et al. Sub-diffractional volume-confined polaritons in the natural hyperbolic material hexagonal boron nitride. *Nat. Commun.* **2014**, *5*, 5221.
(116) Krishnamoorthy, H. N. S.; Jacob, Z.; Narimanov, E.; Kretzschmar, I.; Menon, V. M. Topological transitions in metamaterials. *Science* **2012**, *336*, 205−209.
(117) Berkowitz, M. E.; et al. Hyperbolic Cooper-pair polaritons in planar graphene/cuprate plasmonic cavities. *Nano Lett.* **2021**, *21*, 308−316.
(118) Maccaferri, N.; Zhao, Y.; Isoniemi, T.; Iarossi, M.; Parracino, A.; Strangi, G.; De Angelis, F. Hyperbolic meta-antennas enable full control of scattering and absorption of light. *Nano Lett.* **2019**, *19*, 1851−1859.
(119) Shang, J.; Cong, C.; Wang, Z.; Peimyoo, N.; Wu, L.; Zou, C.; Chen, Y.; Chin, X. Y.; Wang, J.; Soci, C.; Huang, W.; Yu, T. Room-temperature 2D semiconductor activated vertical-cavity surface-emitting lasers. *Nat. Commun.* **2017**, *8*, 543.
(120) Li, Y.; Zhang, J.; Huang, D.; Sun, H.; Fan, F.; Feng, J.; Wang, Z.; Ning, C. Z. Room-temperature continuous-wave lasing from monolayer molybdenum ditelluride integrated with a silicon nanobeam cavity. *Nat. Nanotechnol.* **2017**, *12*, 987−992.
(121) Kern, J.; Trügler, A.; Niehues, I.; Ewering, J.; Schmidt, R.; Schneider, R.; Najmaei, S.; George, A.; Zhang, J.; Lou, J.; Hohenester, U.; Michaelis de Vasconcellos, S.; Bratschitsch, R. Nanoantenna-enhanced light-matter interaction in atomically thin WS_2. *ACS Photonics* **2015**, *2*, 1260−1265.
(122) Duan, J.; Álvarez-Pérez, G.; Voronin, K. V.; Prieto, I.; Taboada-Gutiérrez, J.; Volkov, V. S.; Martín-Sánchez, J.; Nikitin, A. Y.; Alonso-González, P. Enabling propagation of anisotropic polaritons along forbidden directions via a topological transition. *Sci. Adv.* **2021**, *7*, eabf2690.
(123) Taboada-Gutiérrez, J.; et al. Broad spectral tuning of ultra-low-loss polaritons in a van der Waals crystal by intercalation. *Nat. Meter.* **2020**, *19*, 964−968.
(124) Zheng, Z.; Chen, J.; Wang, Y.; Wang, X.; Chen, X.; Liu, P.; Xu, J.; Xie, W.; Chen, H.; Deng, S.; Xu, N. Highly confined and tunable hyperbolic phonon polaritons in van der Waals semiconducting transition metal oxides. *Adv. Mater.* **2018**, *30*, 1705318.
(125) Gjerding, M. N.; Petersen, R.; Pedersen, T. G.; Mortensen, N. A.; Thygesen, K. S. Layered van der Waals crystals with hyperbolic light dispersion. *Nat. Commun.* **2017**, *8*, 320.
(126) Xia, F.; Wang, H.; Xiao, D.; Dubey, M.; Ramasubramaniam, A. Two-dimensional material nanophotonics. *Nat. Photonics* **2014**, *8*, 899−907.
(127) Guo, Q.; Gao, W.; Chen, J.; Liu, Y.; Zhang, S. Line degeneracy and strong spin-orbit coupling of light with bulk bianisotropic metamaterials. *Phys. Rev. Lett.* **2015**, *115*, No. 067402.
(128) Zhao, Y.; Belkin, M. A.; Alù, A. Twisted optical metamaterials for planarized ultrathin broadband circular polarizers. *Nat. Common.* **2012**, *3*, 870.
(129) Burckel, D. B.; Wendt, J. R.; Ten Eyck, G. A.; Ginn, J. C.; Ellis, A. R.; Brener, I.; Sinclair, M. B. Micrometer-scale cubic unit cell 3D metamaterial layers. *Adv. Mater.* **2010**, *22*, 5053−5057.
(130) Liu, Z.; Du, H.; Li, J.; Lu, L.; Li, Z.-Y.; Fang, N. X. Nano-kirigami with giant optical chirality. *Sci. Adv.* **2018**, *4*, eaat4436.
(131) Ra'di, Y.; Grbic, A. Magnet-free nonreciprocal bianisotropic metasurfaces. *Phys. Rev. B* **2016**, *94*, 195432.
(132) Wang, X.; Ptitcyn, G.; Asadchy, V. S.; Díaz-Rubio, A.; Mirmoosa, M. S.; Fan, S.; Tretyakov, S. A. Nonreciprocity in bianisotropic systems with uniform time modulation. *Phys. Rev. Lett.* **2020**, *125*, 266102.
(133) Droulias, S. Chiral sensing with achiral isotropic metasurfaces. *Phys. Rev. B* **2020**, *102*, No. 075119.
(134) Alaee, R.; Albooyeh, M.; Yazdi, M.; Komjani, N.; Simovski, C.; Lederer, F.; Rockstuhl, C. Magnetoelectric coupling in nonidentical plasmonic nanoparticles: theory and applications. *Phys. Rev. B* **2015**, *91*, 115119.
(135) Wang, D.-X.; Lau, P. Y.; Yung, E. K.-N.; Chen, R.-S. Scattering by conducting bodies coated with bi-isotropic materials. *IEEE Trans. Antennas Propag.* **2007**, *55*, 2313−2319.
(136) Sheng, L.; Zhou, X.; Zhong, Y.; Zhang, X.; Chen, Y.; Zhang, Z.; Chen, H.; Lin, X. Exotic photonic spin Hall effect from a chiral interface. *Laser Photonics Rev.* **2023**, *17*, 2200534.
(137) Mobini, E.; Alaee, R.; Boyd, R. W.; Dolgaleva, K. Giant asymmetric second-harmonic generation in bianisotropic metasurfaces based on bound states in the continuum. *ACS Photonics* **2021**, *8*, 3234−3240.
(138) Evlyukhin, A. B.; Tuz, Vl. R.; Volkov, V. S.; Chichkov, B. N. Bianisotropy for light trapping in all-dielectric metasurfaces. *Phys. Rev. B* **2020**, *101*, 205415.
(139) Wu, C.; Arju, N.; Kelp, G.; Fan, J. A.; Dominguez, J.; Gonzales, E.; Tutuc, E.; Brener, I.; Shvets, G. Spectrally selective chiral silicon metasurfaces based on infrared Fano resonances. *Nat. Common.* **2014**, *5*, 3892.
(140) Asadchy, V.; Ra'di, Y.; Vehmas, J.; Tretyakov, S. Functional metamirrors using bianisotropic elements. *Phys. Rev. Lett.* **2015**, *114*, No. 095503.
(141) Hasar, U. C.; Muratoglu, A.; Bute, M.; Barroso, J. J.; Ertugrul, M. Effective constitutive parameters retrieval method for bianisotropic metamaterials using waveguide measurements. *IEEE Trans. Microw. Theory Techn.* **2017**, *65*, 1488−1497.
(142) Ahmed, F.; Tamoor, T.; Hassan, T.; Shoaib, N.; Alomainy, A.; Abbasi, Q. H. Design and development of a multi-functional bi-anisotropic metasurface with ultra-wide out of band transmission. *Sci. Rep.* **2021**, *11*, 24244.
(143) Kang, M.; Zhang, T.; Zhao, B.; Sun, L.; Chen, J. Chirality of exceptional points in bianisotropic metasurfaces. *Opt. Express* **2021**, *29*, 11582−11590.
(144) Lin, B.-Q.; Guo, J.-X.; Chu, P.; Huo, W.-J.; Xing, Z.; Huang, B.-G.; Wu, L. Multiple-band linear-polarization conversion and circular polarization in reflection mode using a symmetric anisotropic metasurface. *Phys. Rev. Appl.* **2018**, *9*, No. 024038.
(145) Asadchy, V. S.; Díaz-Rubio, A.; Tretyakov, S. A. Bianisotropic metasurfaces: physics and applications. *Nanophotonics* **2018**, *7*, 1069−1094.
(146) Yang, F.; Rahmat-Samll, Y. *Surface Electromagnetics with Applications in Antenna, Microwave, And Optical Engineering*; Cambridge University Press, 2019.
(147) Cao, Y.; et al. Correlated insulator behaviour at half-filling in magic-angle graphene superlattices. *Nature* **2018**, *556*, 80−84.
(148) Bistritzer, R.; MacDonald, A. H. Moirébands in twisted doublelayer graphene. *Proc. Natl. Acad. Sci. U. S. A.* **2011**, *108*, 12233−12237.
(149) Zhang, X.; Zhong, Y.; Low, T.; Chen, H.; Lin, X. Emerging chiral optics from chiral interfaces. *Phys. Rev. B* **2021**, *103*, 195405.
(150) Lin, X.; Liu, Z.; Stauber, T.; Gómez-Santos, G.; Gao, F.; Chen, H.; Zhang, B.; Low, T. Chiral plasmons with twisted atomic bilayers. *Phys. Rev. lett.* **2020**, *125*, No. 077401.

https://doi.org/10.1021/acsphotonics.2c01705
ACS Photonics XXXX, XXX, XXX−XXX

(151) Stauber, T.; Low, T.; Gómez-Santos, G. Chiral response of twisted bilayer graphene. *Phys. Rev. Lett.* **2018**, *120*, No. 046801.
(152) Stauber, T.; Low, T.; Gómez-Santos, G. Linear response of twisted bilayer graphene: continuum versus tight-binding models. *Phys. Rev. B* **2018**, *98*, 195414.
(153) Hu, F.; Das, S. R.; Luan, Y.; Chung, T.-F.; Chen, Y. P.; Fei, Z. Real-space imaging of the tailored plasmons in twisted bilayer graphene. *Phys. Rev. Lett.* **2017**, *119*, 247402.
(154) Pfeiffer, C.; Zhang, C.; Ray, V.; Jay Guo, L.; Grbic, A. Polarization rotation with ultra-thin bianisotropic metasurfaces. *Optica* **2016**, *3*, 427−432.
(155) Jing, L.; Lin, X.; Wang, Z.; Kaminer, I.; Hu, H.; Li, E.; Liu, Y.; Chen, M.; Zhang, B.; Chen, H. Polarization shaping of free-electron radiation by gradient bianisotropic metasurfaces. *Laser Photonics Rev.* **2021**, *15*, 2000426.
(156) Tay, F.; Lin, X.; Shi, X.; Chen, H.; Kaminer, I.; Zhang, B. Anomalous free-electron radiation beyond the conventional formation time. *arXiv:2211.14377 [physics.comp-ph]* **2022**, na.
(157) Chen, J. Low-velocity-favored transition radiation. *arXiv:2212.13066 [physics.optics]* **2022**, na.
(158) Dixon, J.; Lawrence, M.; Barton, D. R., III; Dionne, J. Self-isolated raman lasing with a chiral dielectric metasurface. *Phys. Rev. Lett.* **2021**, *126*, 123201.
(159) Pfeiffer, C.; Zhang, C.; Ray, V.; Guo, L. J.; Grbic, A. High performance bianisotropic metasurfaces: asymmetric transmission of light. *Phys. Rev. Lett.* **2014**, *113*, No. 023902.
(160) Sievenpiper, D.; Schaffner, J.; Song, H.; Loo, R.; Tangonan, G. Two-dimensional beam steering using an electrically tunable impedance surface. *IEEE Trans. Antennas Propag.* **2003**, *51*, 2713−2722.
(161) Chen, K.; Feng, Y.; Monticone, F.; Zhao, J.; Zhu, B.; Jiang, T.; Zhang, L.; Kim, Y.; Ding, X.; Zhang, S.; Alù, A.; Qiu, C.-W. A Reconfigurable active Huygens' metalens. *Adv. Mater.* **2017**, *29*, 1606422.
(162) Shalaginov, M. Y.; et al. Design for quality: reconfigurable flat optics based on active metasurfaces. *Nanophotonics* **2020**, *9*, 3505−3534.
(163) Wu, P. C.; Pala, R. A.; Shirmanesh, G. K.; Cheng, W.-H.; Sokhoyan, R.; Grajower, M.; Alam, M. Z.; Lee, D.; Atwater, H. A. Dynamic beam steering with all-dielectric electro-optic III-V multiple-quantum-well metasurfaces. *Nat. Commun.* **2019**, *10*, 3654.
(164) Chen, H.-T.; Padilla, W. J.; Cich, M. J.; Azad, A. K.; Averitt, R. D.; Taylor, A. J. A metamaterial solid-state terahertz phase modulator. *Nat. Photonics* **2009**, *3*, 148−151.
(165) Zeng, B.; Huang, Z.; Singh, A.; Yao, Y.; Azad, A. K.; Mohite, A. D.; Taylor, A. J.; Smith, D. R.; Chen, H.-T. Hybrid graphene metasurfaces for high-speed mid-infrared light modulation and single-pixel imaging. *Light Sci. Appl.* **2018**, *7*, 51.
(166) Cardin, A. E.; Silva, S. R.; Vardeny, S. R.; Padilla, W. J.; Saxena, A.; Taylor, A. J.; Kort-Kamp, W. J. M.; Chen, H.-T.; Dalvit, D. A. R.; Azad, A. K. Surface-wave-assisted nonreciprocity in spatio-temporally modulated metasurfaces. *Nat. Common.* **2020**, *11*, 1469.
(167) Shou, Y.; Feng, Y.; Zhang, Y.; Chen, H.; Qian, H. Deep learning approach based optical edge detection using ENZ layers. *Prog. Electromagn. Res.* **2022**, *175*, 81−89.
(168) Fan, Z.; et al. Homeostatic neuro-metasurfaces for dynamic wireless channel management. *Sci. Adv.* **2022**, *8*, eabn7905.
(169) Huang, M.; Zheng, B.; Cai, T.; Li, X.; Liu, J.; Qian, C.; Chen, H. Machine-learning-enabled metasurface for direction of arrival estimation. *Nanophotonics* **2022**, *11*, 2001−2010.
(170) Ni, Y.; Chen, C.; Wen, S.; Xue, X.; Sun, L.; Yang, Y. Computational spectropolarimetry with a tunable liquid crystal metasurface. *eLight* **2022**, *2*, 23.
(171) Shabanpour, J. Programmable anisotropic digital metasurface for independent manipulation of dual-polarized THz waves based on a voltage-controlled phase transition of VO_2 microwires. *J. Mater. Chem. C* **2020**, *8*, 7189−7199.
(172) Venkatesh, S.; Lu, X.; Saeidi, H.; Sengupta, K. A high-speed programmable and scalable terahertz holographic metasurface based on tiled CMOS chips. *Nat. Electron.* **2020**, *3*, 785−793.
(173) Zhang, X. G.; et al. An optically driven digital metasurface for programming electromagnetic functions. *Nat. Electron.* **2020**, *3*, 165−171.
(174) Li, L.; Jun Cui, T.; Ji, W.; Liu, S.; Ding, J.; Wan, X.; Bo Li, Y.; Jiang, M.; Qiu, C.-W.; Zhang, S. Electromagnetic reprogrammable coding-metasurface holograms. *Nat. Commun.* **2017**, *8*, 197.
(175) Cui, T. J.; Qi, M. Q.; Wan, X.; Zhao, J.; Cheng, Q.; et al. Coding metamaterials, digital metamaterials and programmable metamaterials. *Light: Sci. Appl.* **2014**, *3*, e218.
(176) Qian, C.; Wang, Z.; Qian, H.; Cai, T.; Zheng, B.; Lin, X.; Shen, Y.; Kaminer, I.; Li, E.; Chen, H. Dynamic recognition and mirage using neurometamaterials. *Nat. Commun.* **2022**, *13*, 1694.
(177) Galiffi, E.; et al. Photonics of time-varying media. *Adv. Photon.* **2022**, *4*, No. 014002.
(178) Qian, C.; Zheng, B.; Shen, Y.; Jing, L.; Li, E.; Shen, L.; Chen, H. Deep-learning-enabled self-adaptive microwave cloak without human intervention. *Nat. Photonics* **2020**, *14*, 383−390.
(179) Wang, P.; Zheng, Y.; Chen, X.; Huang, C.; Kartashov, Y. V.; Torner, L.; Konotop, V. V.; Ye, F. Localization and delocalization of light in photonic Moiré lattices. *Nature* **2020**, *577*, 42−46.
(180) Sunku, S. S.; et al. Photonic crystals for nano-light in Moiré graphene superlattices. *Science* **2018**, *362*, 1153−1156.
(181) Pfeiffer, C.; Grbic, A. Bianisotropic metasurfaces for optimal polarization control: analysis and synthesis. *Phys. Rev. Appl.* **2014**, *2*, No. 044011.
(182) Shen, L.; Lin, X.; Shalaginov, M. Y.; Low, T.; Zhang, X.; Zhang, B.; Chen, H. Broadband enhancement of on-chip single-photon extraction via tilted hyperbolic metamaterials. *Appl. Phys. Rev.* **2020**, *7*, No. 021403.
(183) Zhong, Y.; Lin, X.; Jiang, J.; Yang, Y.; Liu, G.; Xue, H.; Low, T.; Chen, H.; Zhang, B. Toggling near-field directionality via polarization control of surface waves. *Laser Photonics Rev.* **2021**, *15*, 2000388.
(184) Lin, X.; Easo, S.; Shen, Y.; Chen, H.; Zhang, B.; Joannopoulos, J. D.; Soljačić, M.; Kaminer, I. Controlling Cherenkov angles with resonance transition radiation. *Nat. Phys.* **2018**, *14*, 816−821.
(185) Wang, X.-R.; Wang, X.-B.; Ren, H.; Wu, N.-S.; Wu, J.-W.; Su, W.-M.; Han, Y.-L.; Xu, S. Optically transparent microwave shielding hybrid film composited by metal mesh and graphene. *Prog. Electromagn. Res.* **2021**, *170*, 187−197.
(186) Jiang, J.; Lin, X.; Zhang, B. Broadband negative refraction of highly squeezed hyperbolic polaritons in 2D materials. *Research* **2018**, *2018*, 2532819.
(187) Li, J. I. A.; Taniguchi, T.; Watanabe, K.; Hone, J.; Dean, C. R. Excitonic superfluid phase in double bilayer graphene. *Nat. Phys.* **2017**, *13*, 751−755.
(188) Hu, G.; Krasnok, A.; Mazor, Y.; Qiu, C.-W.; Alù, A. Moiré hyperbolic metasurfaces. *Nano Lett.* **2020**, *20*, 3217.
(189) Chen, M.; Lin, X.; Dinh, T. H.; Zheng, Z.; Shen, J.; Ma, Q.; Chen, H.; Jarillo-Herrero, P.; Dai, S. Configurable phonon polaritons in twisted α-MoO_3. *Nat. Mater.* **2020**, *19*, 1307−1311.
(190) Zheng, Z.; Sun, F.; Huang, W.; Jiang, J.; Zhan, R.; Ke, Y.; Chen, H.; Deng, S. Phonon polaritons in twisted double-layers of hyperbolic van der Waals crystals. *Nano Lett.* **2020**, *20*, 5301−5308.
(191) Hu, G.; et al. Topological polaritons and photonic magic angles in twisted α-MoO_3 bilayers. *Nature* **2020**, *582*, 209−213.
(192) Ribeiro-Palau, R.; Zhang, C.; Watanabe, K.; Taniguchi, T.; Hone, J.; Dean, C. R. Twistable electronics with dynamically rotatable heterostructures. *Science* **2018**, *361*, 690−693.
(193) Choi, Y.; et al. Correlation-driven topological phases in magic-angle twisted bilayer graphene. *Nature* **2021**, *589*, 536−541.
(194) Bapat, A.; Dixit, S.; Gupta, Y.; Low, T.; Kumar, A. Gate tunable light-matter interaction in natural biaxial hyperbolic van der Waals heterostructures. *Nanophotonics* **2022**, *11*, 2329−2340.
(195) Álvarez-Pérez, G.; González-Morán, A.; Capote-Robayna, N.; Voronin, K. V.; Duan, J.; Volkov, V. S.; Alonso-González, P.; Nikitin,

https://doi.org/10.1021/acsphotonics.2c01705
ACS Photonics XXXX, XXX, XXX−XXX

A. Y. Active tuning of highly anisotropic phonon polaritons in van der Waals crystal slabs by gated graphene. *ACS Photonics* **2022**, *9*, 383−390.
(196) Hu, H.; et al. Doping-driven topological polaritons in graphene/α-MoO_3 heterostructures. *Nat. Nanotechnol.* **2022**, *17*, 940−946.
(197) Lou, B.; Zhao, N.; Minkov, M.; Guo, C.; Orenstein, M.; Fan, S. Theory for twisted bilayer photonic crystal slabs. *Phys. Rev. Lett.* **2021**, *126*, 136101.
(198) Chen, J.; Lin, X.; Chen, M.; Low, T.; Chen, H.; Dai, S. A perspective of twisted photonic structures. *Appl. Phys. Lett.* **2021**, *119*, 240501.
(199) Liu, X. Tunable spin-polarized correlated states in twisted double bilayer graphene. *Nature* **2020**, *583*, 221−225.
(200) Zhang, L.; Gogna, R.; Burg, W.; Tutuc, E.; Deng, H. Photonic-crystal exciton-polaritons in monolayer semiconductors. *Nat. Common.* **2018**, *9*, 713.
(201) Liu, W.; Ji, Z.; Wang, Y.; Modi, G.; Hwang, M.; Zheng, B.; Sorger, V. J.; Pan, A.; Agarwal, R. Generation of helical topological exciton-polaritons. *Science* **2020**, *370*, 600−604.
(202) Jiang, Y.; Lin, X.; Chen, H. Directional polaritonic excitation of circular, Huygens and Janus dipoles in graphene-hexagonal boron nitride heterostructures. *Prog. Electromagn. Res.* **2021**, *170*, 169−176.
(203) Hu, H.; Lin, X.; Wong, L. J.; Yang, Q.; Liu, D.; Zhang, B.; Luo, Y. Surface Dyakonov-Cherenkov radiation. *eLight* **2022**, *2*, 2.
(204) Zhong, Y.; Cai, T.; Low, T.; Chen, H.; Lin, X. Optical interface engineering with on-demand magnetic surface conductivities. *Phys. Rev. B* **2022**, *106*, No. 035304.

https://doi.org/10.1021/acsphotonics.2c01705
ACS Photonics XXXX, XXX, XXX−XXX